AD-A011 491

BOUND-BOUND RADIATION/COLLISIONAL-
RADIATIVE RECOMBINATION IN OXYGEN
AND NITROGEN PLASMAS

Larry A. Jones

Naval Research Laboratory

190131

ADA011491

DNA 3565F

BOUND-BOUND RADIATION/COLLISIONAL-RADIATIVE RECOMBINATION IN OXYGEN AND NITROGEN PLASMAS

Naval Research Laboratory
Washington, D.C 20375

13 February 1975

Final Report for Period 1 January 1974—31 December 1974
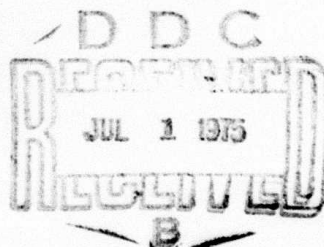
CONTRACT No. DNA MIPR 75-580

APPROVED FOR PUBLIC RELEASE;
DISTRIBUTION UNLIMITED.

D D C
JUL 1 1975
RECEIVED
B

Prepared for

Director

DEFENSE NUCLEAR AGENCY

Washington, D. C. 20305

54

REPORT DOCUMENTATION PAGE		READ INSTRUCTIONS BEFORE COMPLETING FORM
1. REPORT NUMBER DNA 3565F	2. GOVT ACCESSION NO.	3. RECIPIENT'S CATALOG NUMBER
4. TITLE (and Subtitle) BOUND-BOUND RADIATION/COLLISIONAL-RADIATIVE RECOMBINATION IN OXYGEN AND NITROGEN PLASMAS		5. TYPE OF REPORT & PERIOD COVERED Final Report for Period 1 Jan 74—31 Dec 74
		6. PERFORMING ORG. REPORT NUMBER
7. AUTHOR(s) Larry A. Jones		8. CONTRACT OR GRANT NUMBER(s) DNA MIPR 75-580
9. PERFORMING ORGANIZATION NAME AND ADDRESS Naval Research Laboratory Washington, D.C. 20375		10. PROGRAM ELEMENT, PROJECT, TASK AREA & WORK UNIT NUMBERS NWED Subtask M99QAXHI002-06
11. CONTROLLING OFFICE NAME AND ADDRESS Director Defense Nuclear Agency Washington, D.C. 20305		12. REPORT DATE 13 February 1975
		13. NUMBER OF PAGES 54
14. MONITORING AGENCY NAME & ADDRESS(if different from Controlling Office) Defense Advanced Research Projects Agency 1400 Wilson Boulevard Arlington, Virginia 22209		15. SECURITY CLASS (of this report) UNCLASSIFIED
		15a. DECLASSIFICATION/DOWNGRADING SCHEDULE

16. DISTRIBUTION STATEMENT (of this Report)

Approved for public release; distribution unlimited.

17. DISTRIBUTION STATEMENT (of the abstract entered in Block 20, if different from Report)

19. KEY WORDS (Continue on reverse side if necessary and identify by block number)

Plasma Physics
Collisional-Radiative Recombination
Nitrogen and Oxygen Plasmas
Bound-Bound Radiation

20. ABSTRACT (Continue on reverse side if necessary and identify by block number)

Number densities of several excited states of atomic oxygen and nitrogen have been measured in the decaying non-thermal plasma of a θ-pinch afterglow. The spatial variation of the electron density and temperature as a function of time after the initiation of main bank discharge have also been measured to facilitate a comparison of excited state number densities with model calculations. Measurements of the atomic oxygen excited states indicate that quintet to triplet spin exchange collisions and doubly excited states must be included in the model. The measured

DD FORM 1473 1 JAN 73 EDITION OF 1 NOV 65 IS OBSOLETE

PRICES SUBJECT TO CHANGE

10. PROGRAM ELEMENT, PROJECT, TASK AREA & WORK UNIT
     NUMBERS (Continued).

DARPA Order 1433, Amendment 12, Program Code 5E50, Program Element
Code 62301E.

20. ABSTRACT (Continued).

populations of the excited atomic nitrogen states agree well with those calculated at
high density ($N_e \cong 10^{14}$ cm^{-3}) but disagree badly at lower densities ($N_e \approx 10^{12}$ cm^{-3}).
The discrepancies seem to be real since they are larger than expected measurement
uncertainty.

TABLE OF CONTENTS

LIST OF ILLUSTRATIONS

LIST OF ILLUSTRATIONS (Continued).

LIST OF ILLUSTRATIONS (Continued).

I. INTRODUCTION

For several years theoretical models (References 1 and 2), which predict the bound-bound infrared (1-10μm) emissivity of an atmospheric-type plasma, have been used with little experimental comparison. These calculations, done at Naval Research Laboratory (NRL) and other places, use a collisional-radiative model (References 3 through 7) to calculate the number densities of the excited states of oxygen and nitrogen atoms submerged in a plasma. From the number densities of the excited states of an atom, one can easily calculate the bound-bound optically thin emission in any spectral region from (Reference 8)

$$I = \frac{\hbar\omega}{4\pi} A_{ul} N_u L_u . \tag{1}$$

where I is the intensity of the radiation, ω is the angular frequency of the radiation emitted, A_{ul} is the atomic transition probability, N_u is the number density of the excited state, and L is the length of the plasma.

The purpose of this experiment is to provide a check of the various assumptions which go into the theoretical models mentioned above. To do this, the number densities of selected excited states of oxygen and nitrogen atoms submerged in a non-equilibrium plasma have been measured. This was done by measuring the absolute intensity of bound-bound visible radiation emitted by atoms undergoing transitions from the state of interest to some other state (References 9 through 11). This combined with good plasma diagnostics to measure the plasma length is then used along with equation (1) to give the excited state number densities. Of course the spatial development of the plasma parameters, electron density and temperature, must also be known so that an unambiguous comparison of the experimental number densities can be made with those generated by the computer programs.

The atmospheric simulation computer programs were originally developed to investigate the collisional-radiative recombination of a low electron density ($N_e \approx 10^6 - 10^{10}$ cm^{-3}) plasma with a temperature of a few tenths of an electron volt. In practice, it is difficult to detect the line radiation emitted by a plasma at these low densities and temperatures when the size of the plasma is restricted to laboratory dimensions. For this reason, our measurements were performed at electron densities between 10^{12} and 10^{14} cm^{-3} with temperatures between 0.3

and 1.5 eV. It should be noted that the assumptions made when developing the model codes should still be valid in this region thereby making a comparison possible.

The next section will describe the θ-pinch used as a plasma source in this experiment. After that the oxygen diagnostics and results will be discussed in total. Then the nitrogen diagnostics and results will be presented. The final section will be a summary of results and some comparisons between the two experiments.

II. APPARATUS

The plasma source used for this experiment was a θ-pinch. A hybrid schematic is shown in Figure 1. The tube is made of quartz and is 137 cm long with an inside diameter of 9 cm. The single-turn θ-pinch coil is 80 cm long and has a slot in the center, for side-on viewing, which is not shown in the diagram. The ambient gas in the discharge tube is preionized by discharging a free ringing 0.126 μF, 20 kV capacitor through small side coils. The plasma is then further heated by discharging a low inductance free ringing 1.5 μF, 20 kV capacitor through the single-turn main coil. Finally the high inductance 250 μF, 20 kV main bank is discharged through the single-turn main coil. This bank is clamped and has a quarter period of about 18 μsec with an e-folding decay time of about 200 μsec. In this manner, a slowly decaying plasma is produced with initial conditions of electron density $\sim 10^{15}$ cm^{-3} and electron temperature ~ 3 eV. The large initial field ~ 9 kG produced by the main bank discharge helps isolate the walls of the quartz tube from the hot early plasma. This helps to improve the purity of the plasma. The longevity of the magnetic field produced by the main bank discharge improves the radial homogeneity of the plasma by slowing down the radial loss rate.

III. OXYGEN MEASUREMENTS

A. Diagnostics

The ambient fill gas used throughout this part of the experiment was pure O_2 at a pressure of 10 mTorr. The first diagnostic done on the plasma was to take the time-integrated spectrum shown in Figure 2. The lower spectrum is that of the plasma emission observed down the axis of the θ-pinch tube with a one-meter spectrograph. The top spectrum is of a krypton lamp used for wavelength calibration. All the lines in the spectrum emitted by the plasma have been identified as originating from atomic oxygen, ionized oxygen or hydrogen atoms, indicating a low impurity level.

6

MAIN BANK

SPARK GAP SWITCH

INDUCTOR

PREHEATER

TO CHARGING UNIT

250 μF 17 kV

CROWBAR SWITCH

20 μF 16 kV

SPARK GAP SWITCH

TO CHARGING UNIT

PRE - PREHEATER

SPARK GAP SWITCH

0.12 μF 16 kV

TO CHARGING UNIT

COLLECTOR PLATES

TUBE

PRE - PREHEATER COIL

MAIN COIL

PRE - PREHEATER COIL
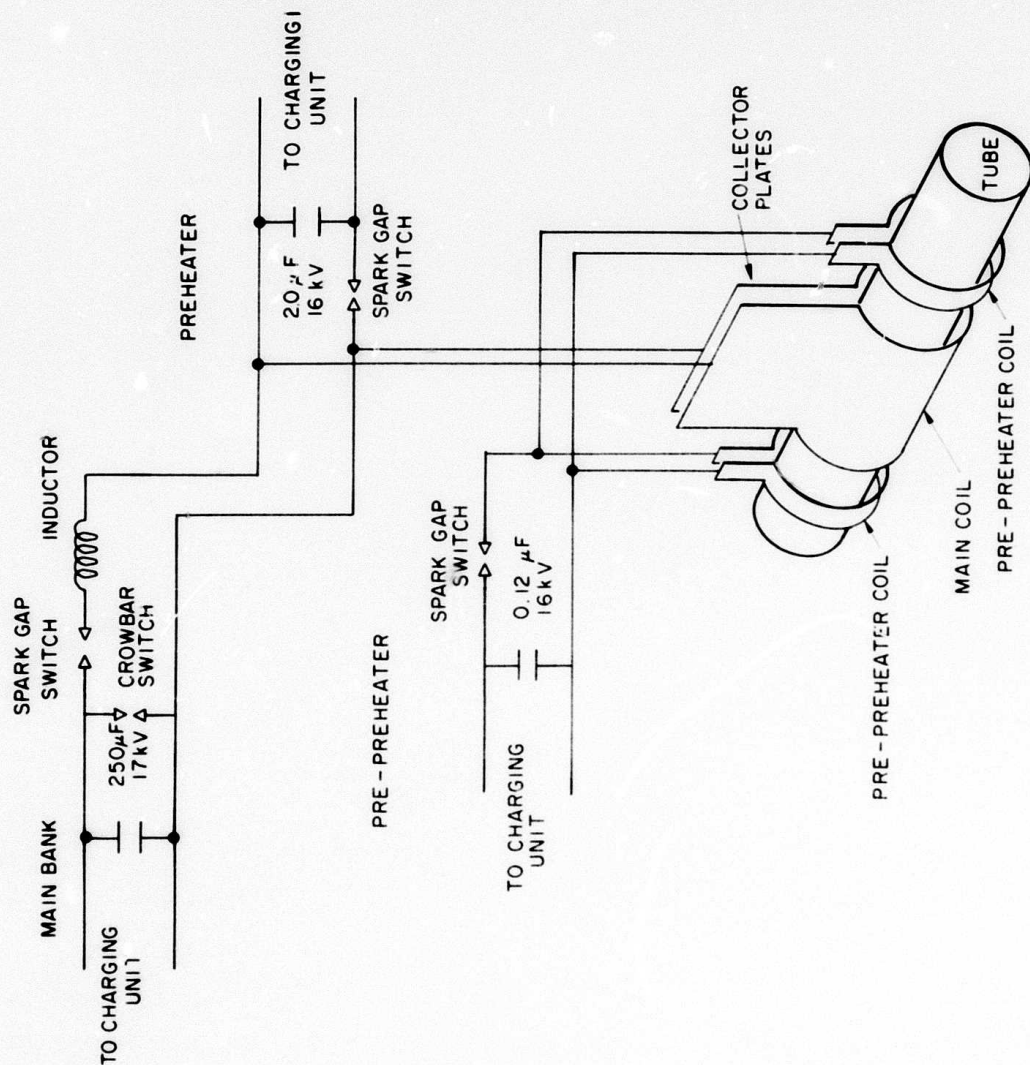
Figure 1. Hybrid schematic of the 50 kJ θ-pinch used as a plasma source.

Figure 2. Time integrated spectrum of visible light emitted from the oxygen plasma.

The next thing done was to study the time evolution of an atomic oxygen line and an ionized oxygen line. This was done using a photomultiplier tube and a one-meter monochromator. A plot of the relative intensities of these two species, versus time after initiation of main bank discharge is shown in Figure 3. It is clear that although the emission from ionized oxygen dominates the spectrum at early times the atomic oxygen emission will be the only emission at late times.

Since these preliminary diagnostics indicated that a slowly decaying neutral oxygen plasma had been generated at later times, more detailed diagnostics were undertaken. A Langmuir (References 12 through 20) probe system was built in order to measure the ion density and electron temperature of the plasma as a function of space and time. A schematic of the Langmuir probe setup is shown in Figure 4. The oscillator is a free-running sawtooth generator with adjustable frequency, gain, and voltage zero level. A free running oscillator has an advantage over a single pulsed system in that the probe tends to be cleaned by the large currents drawn in the hot, dense early discharge. The voltage applied between the electrodes is measured directly while the current flowing is found by the voltage drop across a known resistor. Both voltages are measured differentially so that the probe is free to float at the plasma potential.

A picture of the equal area double probe used for most of the work presented here is shown in Figure 5. The two electrodes of the probe are made from tungsten wire 0.040 inches in diameter and about 5 mm long. The electrodes are placed ~ 2 mm apart which is the approximate spatial resolution of the probe. The electrodes are mounted on a piece of bent pyrex tubing. The pyrex tube lies in the bottom of the θ-pinch tube and by pulling it in and out axial variations of ion density and electron temperature can be measured. Different radial positions can be investigated by rotating the pyrex tube.

A typical double probe trace is shown in Figure 6. The upper trace is the voltage applied by the ramp generator between the double probe electrodes. The lower trace is proportional to the current flowing through the electrodes of the probe. As can be seen, there is a saturation of the current. From the level at which the current saturates I_{isat} one can determine the ion density N_i from

$$N_i = \frac{1}{K} \frac{I_{isat}}{eA_p} \left(\frac{M_i}{kT_e} \right)^{1/2} , \qquad (2)$$

where e is the charge on an electron, A_p is the probe area, M_i is the ion mass, k is Boltzmann's constant, T_e is the electron temperature, and K is a constant

9
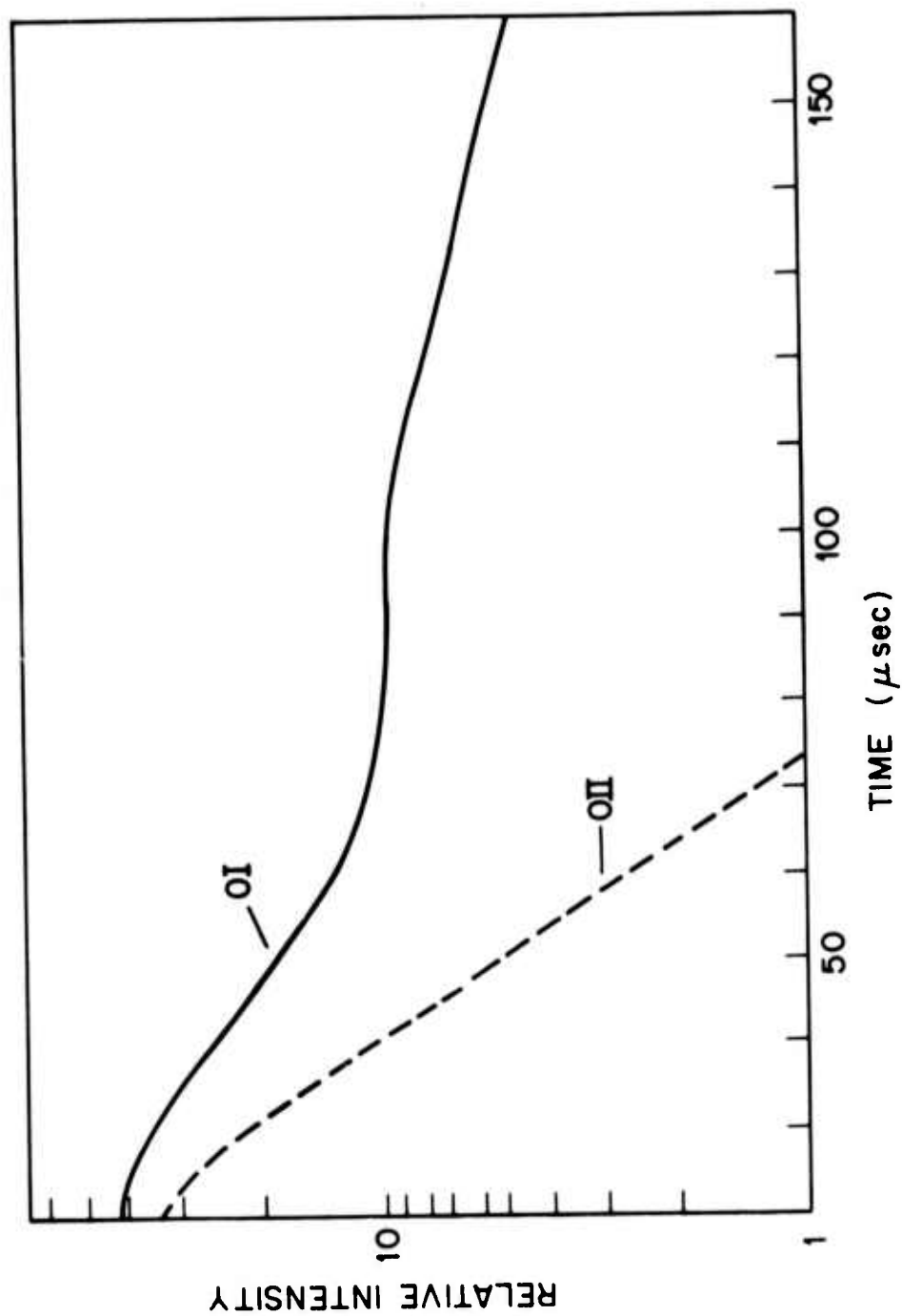
Figure 3. The time development of the emission from neutral oxygen, OI, and ionized oxygen, OII, as a function of time after the initiation of main bank discharge.

10
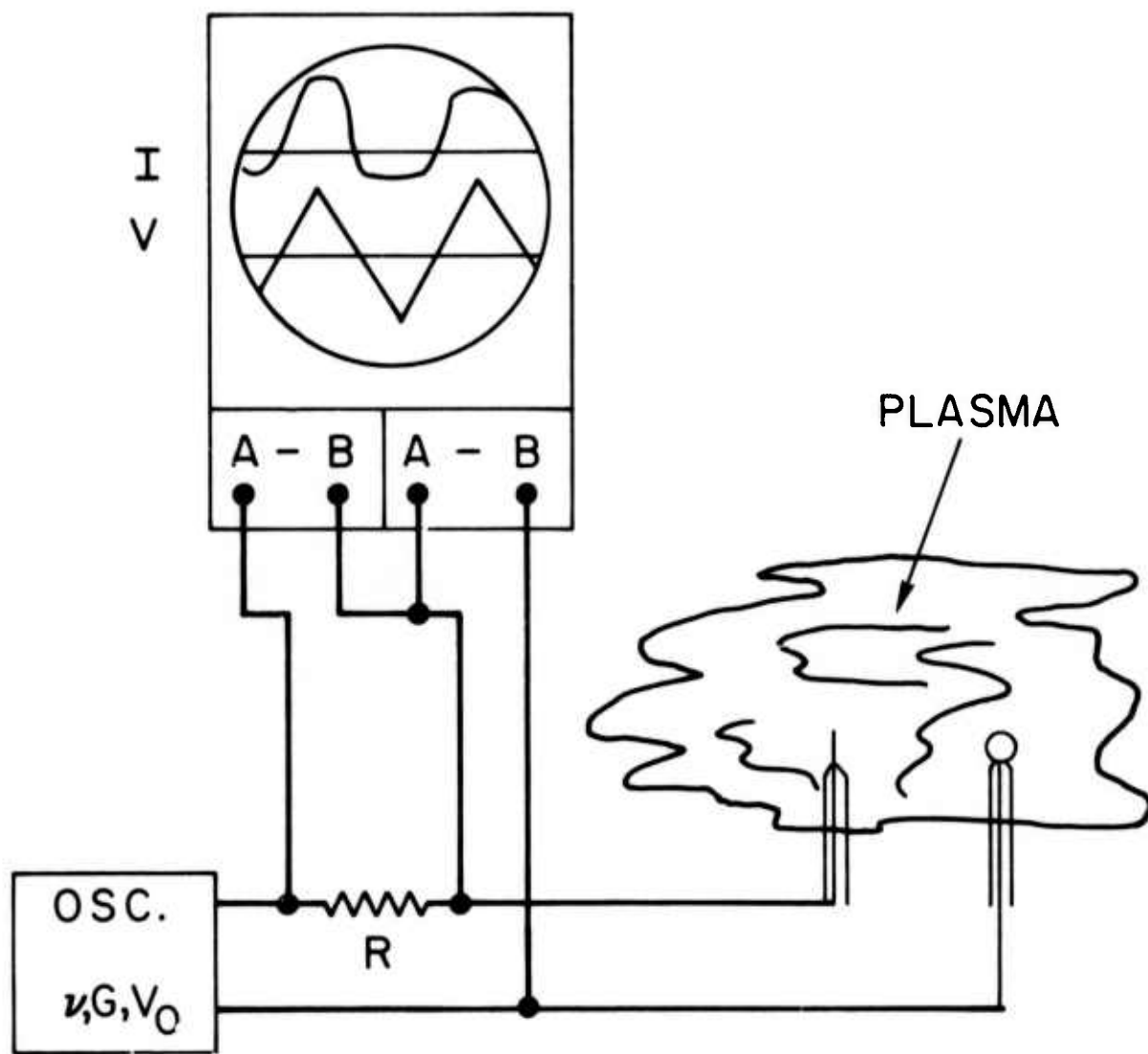
Figure 4. A schematic of the apparatus used to make Langmuir probe measurements.
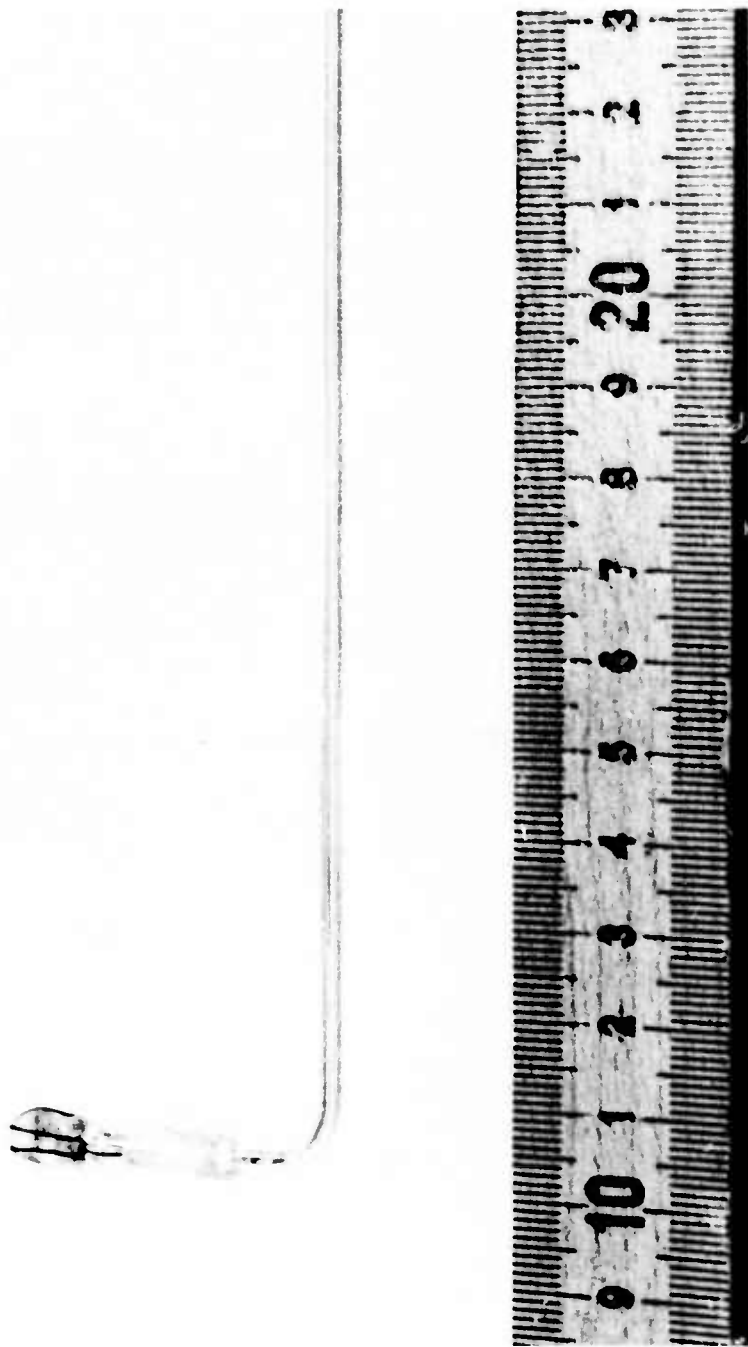
Figure 5. The equal area double probe showing the two tungsten probe electrodes and a portion of the long pyrex tube upon which it is mounted.

12
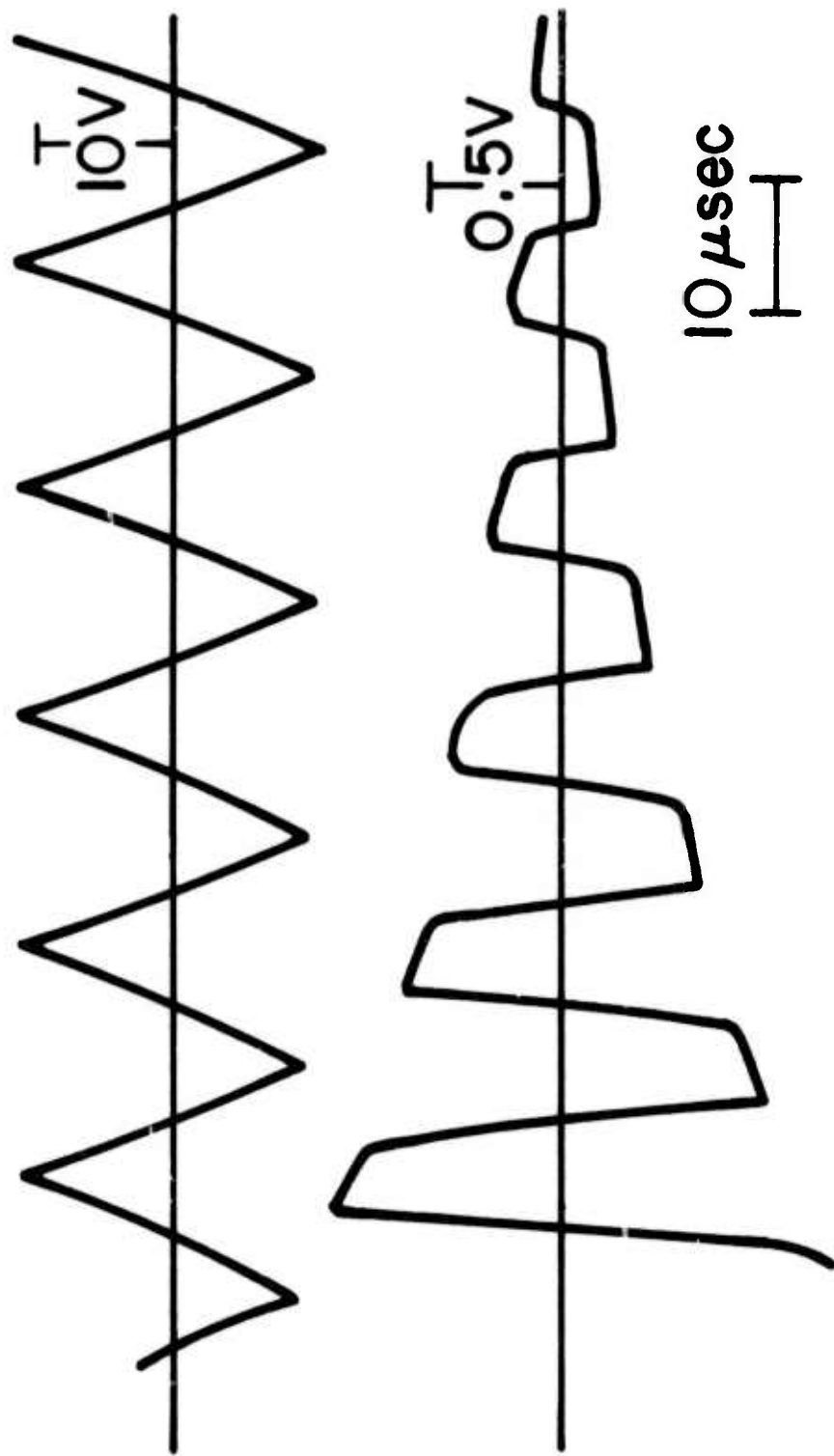
Figure 6. A typical double probe trace showing the voltage applied across the two electrodes on the upper trace and the current flowing through the electrodes on the lower trace. The current is measured by measuring the voltage drop across a known resistor.

13

chosen to be 0.55 as in Reference 16. In our plasma the assumption of quasi-neutrality should be good and thus the ion density should equal the electron density N_e. The electron temperature, T_e is obtained from the rate of change of current, I, with respect to voltage V, when the voltage is zero as given by

$$kT_e = e\left(\frac{dV}{dI}\right)_{V\,=\,0} \frac{I_{isat}}{2} \quad . \tag{3}$$

Three radial scans and many axial scans were done, and it was found that the temperature was not a function of position in the plasma only of time. The electron density on the other hand was found to vary spatially and temporally. Three radial scans at the coil center, 44 cm along the axis from the coil center, and 60.5 cm along the axis from the coil center are shown in Figures 7 through 9. These are plots of the ion saturation current in amps (proportional to the electron density) versus radial position from the tube axis at various times after initiation of the main bank discharge. These plots show a flat electron density distribution over the central 4 cm of the tube. This means that no correction need be made for radial inhomogeneities as long as the light collection optics is stopped down to look at only the central 4 cm of the plasma.

A plot of ion saturation current versus axial position at various times after initiation of main bank discharge is shown in Figure 10. Zero is at the center of the single turn θ-pinch coil, and the end wall is at the end of the quartz tube. In this case, there is an inhomogeneity and a correction must be made for it since our absolute light intensity measurements will be made looking axially down the tube. Since the plasma line radiation intensity is approximately proportional to the square of the electron density (N_e^2), the easiest thing to do is integrate N_e^2 along the axis of the tube. One can relate this integral to the square of the electron density on axis, at the coil center, by choosing an effective length (ℓ_{eff}) which when multiplied by N_e^2 on axis at the coil center will give the value of the integral. A plot of ℓ_{eff} versus time is shown in Figure 11. The dashed line at ~140 cm is the true length of the tube. Thus all the homogeneity corrections are lumped into an effective length, and from now on the electron density on axis in the center of the coil will be the only other parameter necessary to do the radiation transfer for our optically thin plasma. The electron density and temperature were measured on axis at the coil center as a function of time. Results from these measurements will be compared later with similar results from Thomson scattering measurements in Figures 14 and 15.

DENSITY VS. RADIAL POSITION AT VARIOUS TIMES AT CENTER OF COIL
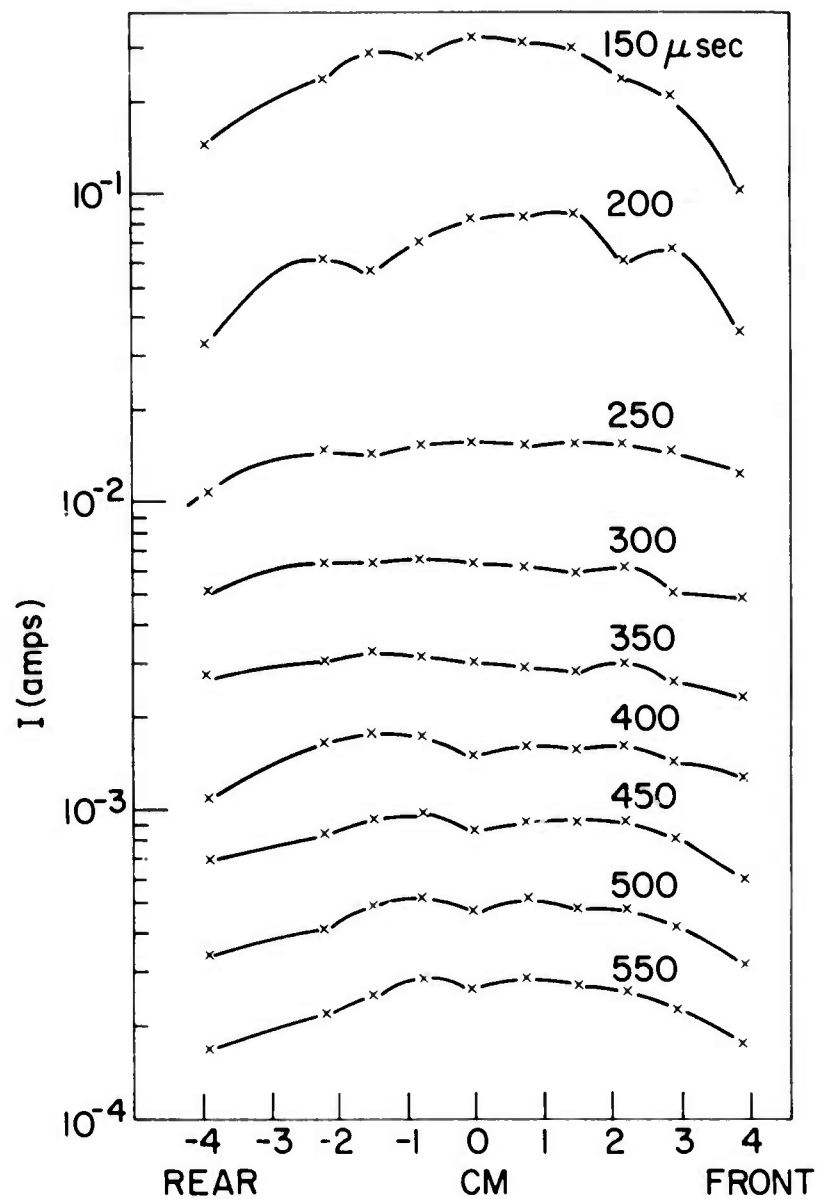
Figure 7. Scan of ion saturation current versus radial position as a function of time after initiation of main bank discharge. These scans were taken in the oxygen plasma in the mid-plane of the single turn θ-pinch coil.

DENSITY VS. RADIAL POSITION AT VARIOUS TIMES
44 cm FROM CENTER OF COIL
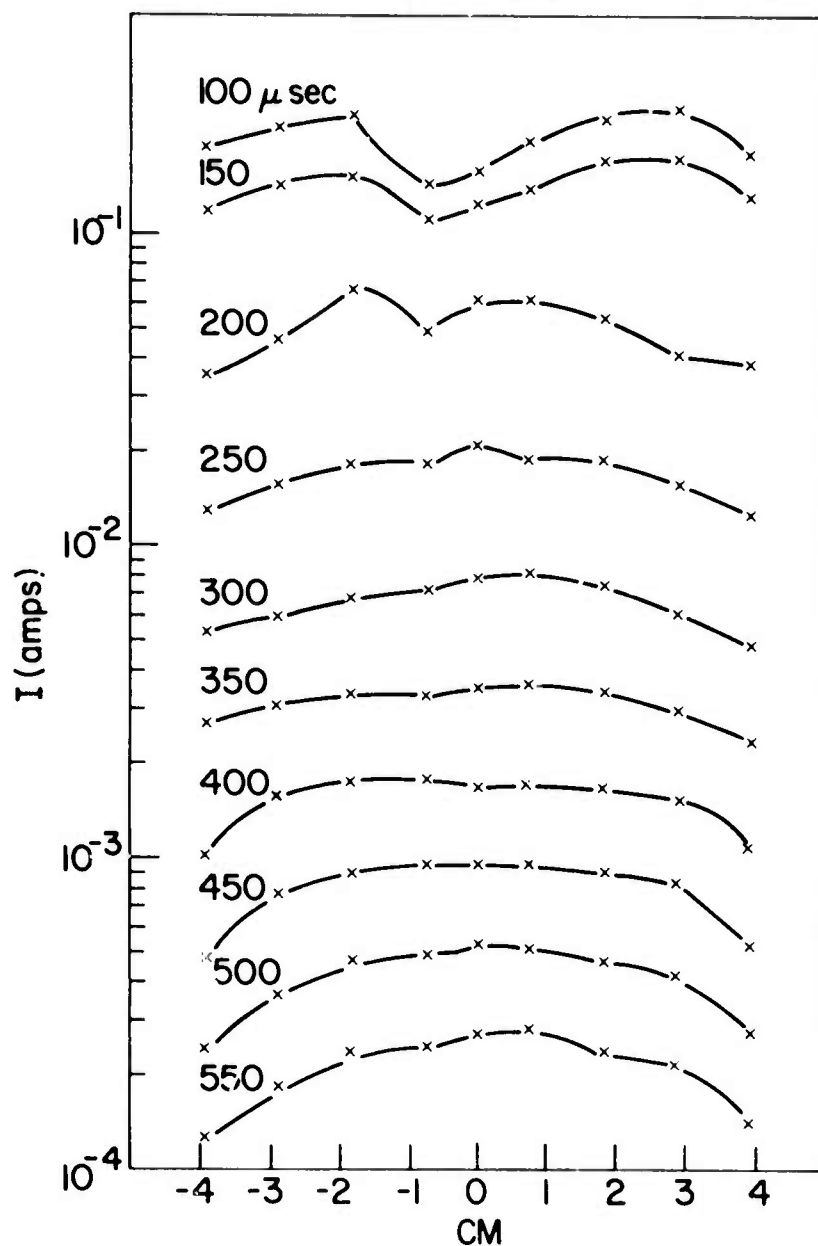
Figure 8. Scan of ion saturation current versus radial position as a function of time after initiation of main bank discharge. These radial scans were taken 44 cm down the tube axis from the mid-plane of the single turn θ-pinch coil.

16

DENSITY VS. RADIAL POSITION AT VARIOUS TIMES
60.5 cm FROM CENTER OF COIL
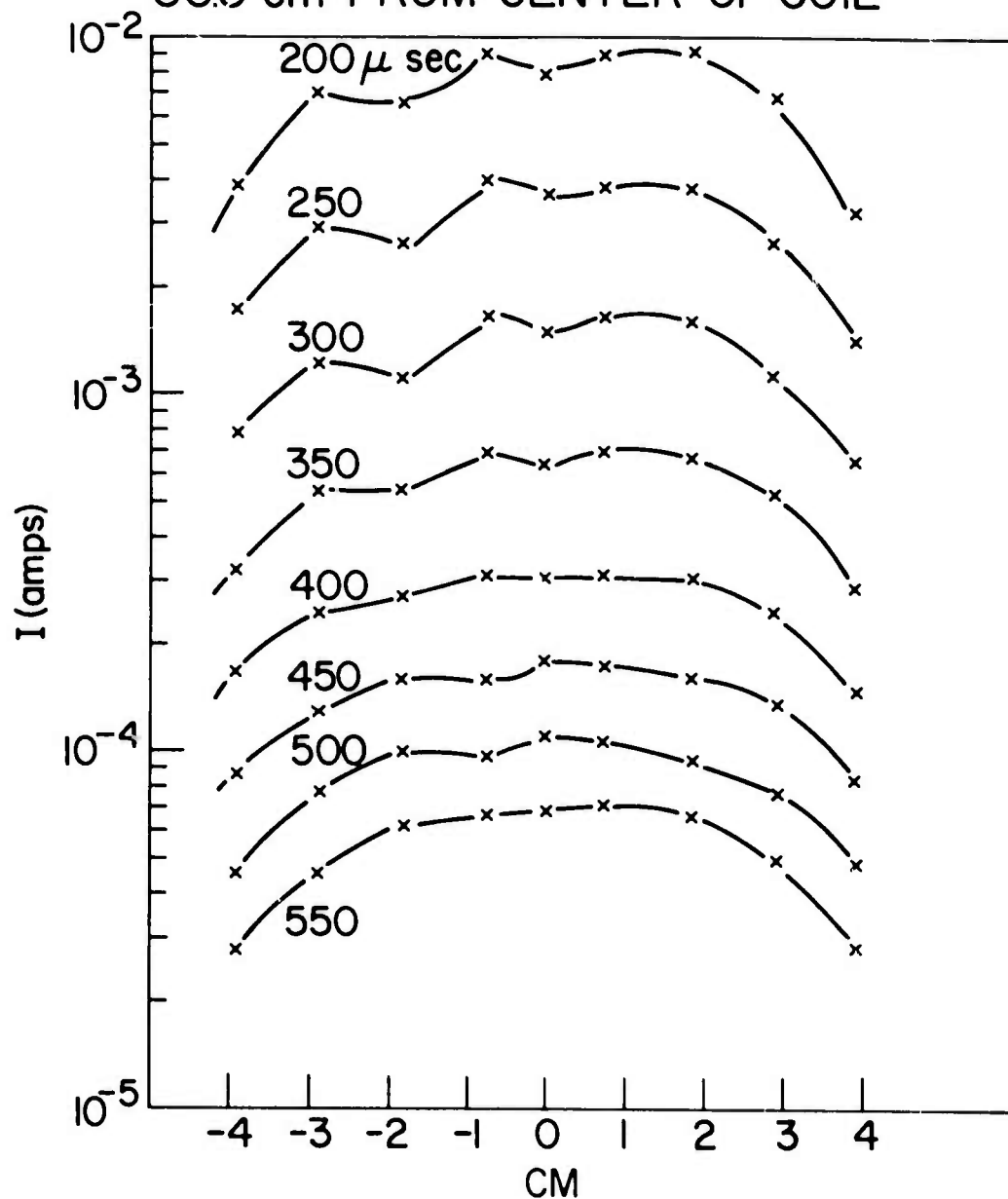
Figure 9. Scan of ion saturation current versus radial position as a
function of time after initiation of main bank discharge.
These radial scans were taken 60.5 cm down the tube
axis from the mid-plane of the single turn θ-pinch coil.

17

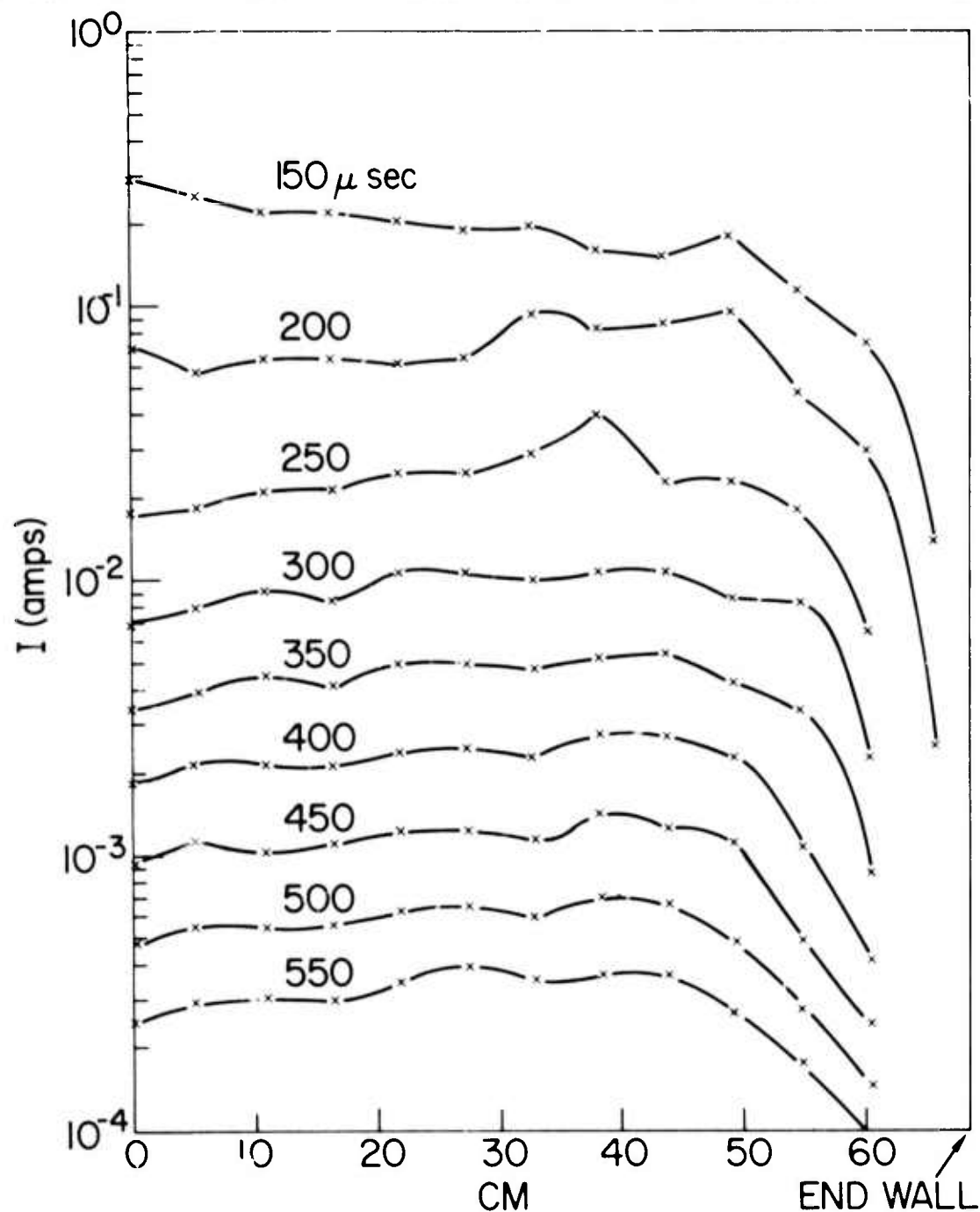# DENSITY VS. AXIAL POSITION AT VARIOUS TIMES

Figure 10. A plot of ion saturation current versus axial position for the oxygen plasma at various times after the initiation of main bank discharge.
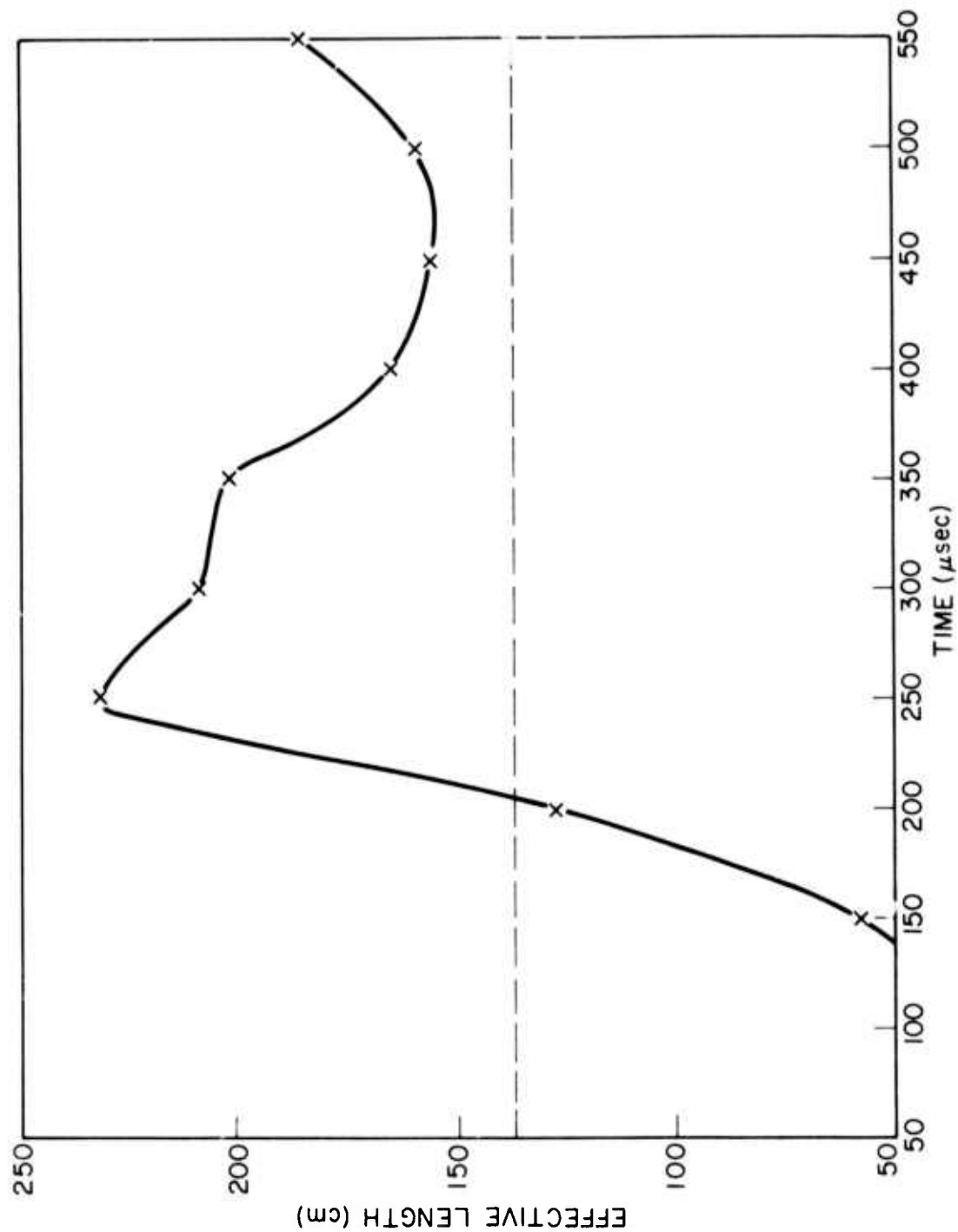
18

Figure 11. A graph showing the variation of the effective length of the oxygen plasma as a function of time. The dashed line is the length of the quartz containment tube.

19

The apparatus used to do Thomson scattering (References 21 and 22) is shown in Figure 12. The 150 MW ruby laser was focused on axis in the center of the coil. The scattered light was viewed at a right angle to the incident beam through a slot in the single-turn main coil. The scattered light was detected by a photomultiplier after being dispersed by a one-meter monochromator. Because of the reproducibility of the θ-pinch, we were able to scan the scattered light profile on a shot-to-shot basis. The central 15 Å of the scattered light profile was not scanned since the stray light level was significant in this region. A typical scattered light profile is shown in Figure 13. This is a plot of relative intensity versus wavelength taken at 94 μsec after initiation of main bank discharge. The temperature is obtained from the half width of the profile while the electron density can be obtained from the absolute total intensity of the scattered light. The absolute total intensity of the scattered light was found by calibrating the photo-detection system using Rayleigh scattering from molecular oxygen.

The original thought behind doing both Langmuir probe and Thomson scattering diagnostics was to use the Langmuir probe as a relative electron density measure. This we could calibrate at early times in the discharge by doing Thomson scattering at one spatial position (on axis at coil), and if necessary all the Langmuir probe data could be multiplied by some constant factor to make it agree with Thomson scattering. As can be seen from the plot of electron density versus time after initiation of main bank discharge, shown in Figure 14, this procedure was unnecessary. Similar agreement was found between the two diagnostic techniques when the electron temperature was measured. A plot of electron temperature versus time after initiation of main bank discharge is shown in Figure 15.

B. Results

A schematic of the apparatus used to make absolute intensity measurements of the visible bound-bound radiation of oxygen is shown in Figure 16. Measurements are made by looking axially down the tube. The aperture stop at the first lens eliminates the need for radial inhomogeneity corrections as discussed in the diagnostics section. The mechanical shutter prevents light emitted by the plasma at early times from saturating the photomultiplier tube which has a high gain for detecting weak signals. Calibration of the detection system is done in situ using a standard tungsten lamp. Absolute intensity measurements were made on eight visible lines of the neutral oxygen spectrum. These line wavelengths along with the transitions (Reference 23) from which they are emitted and other atomic information is given in Table 1.

20
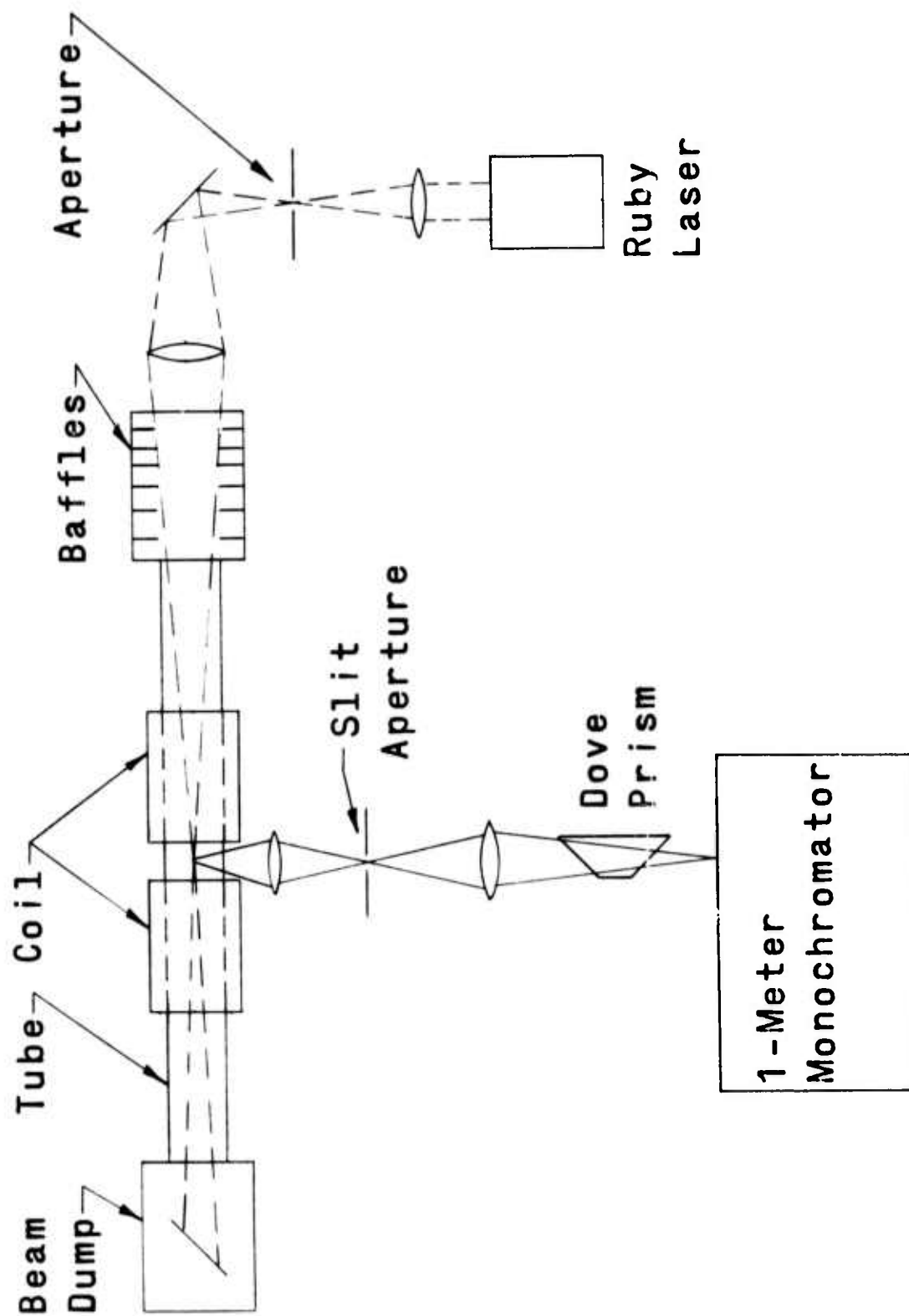
Figure 12. A schematic representation of the Thomson scattering apparatus used to measure electron temperature and density of the plasma in coil mid-plane on axis.

21
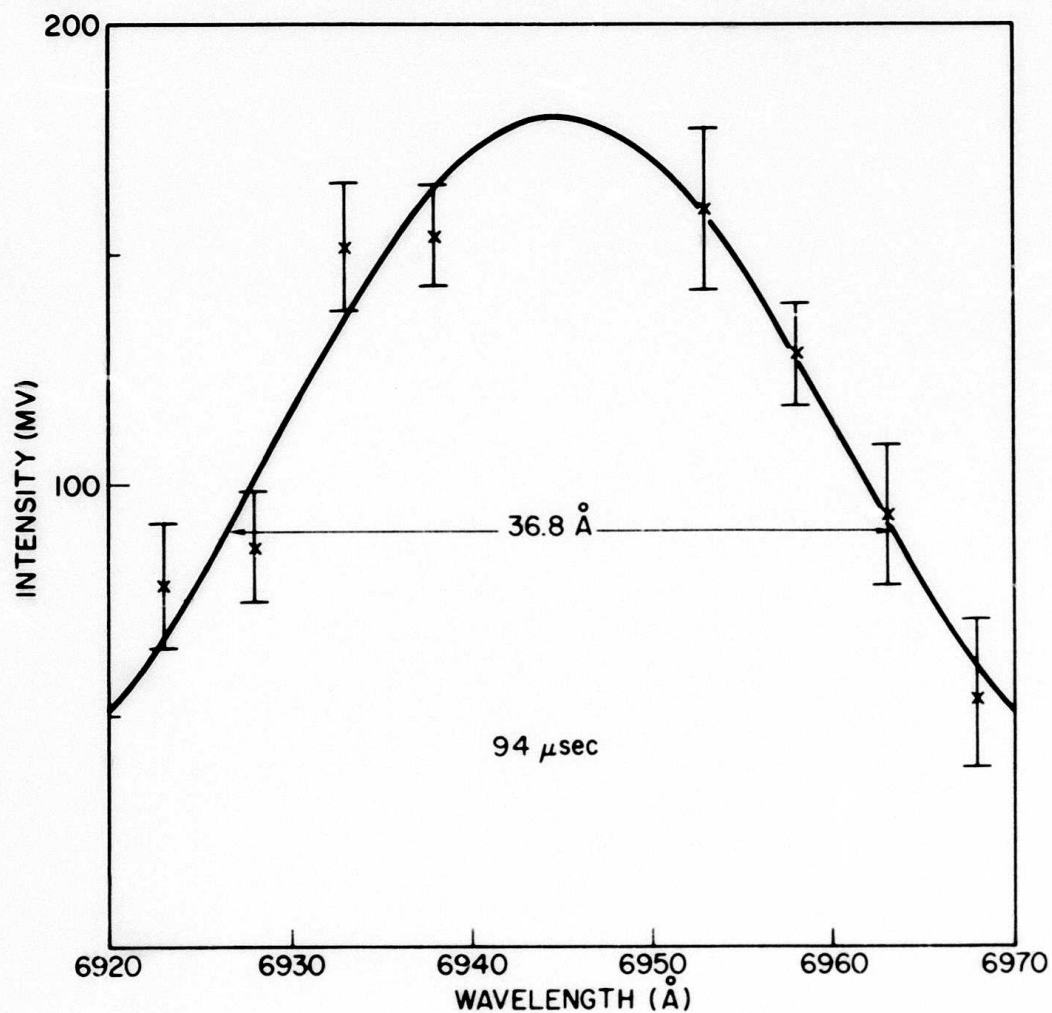
Figure 13. A typical scattered light profile shown fit via least squares to a Gaussian (solid line). The error bars represent the scatter of four different shots. This particular example was taken 94 μsec after initiation of main bank discharge.
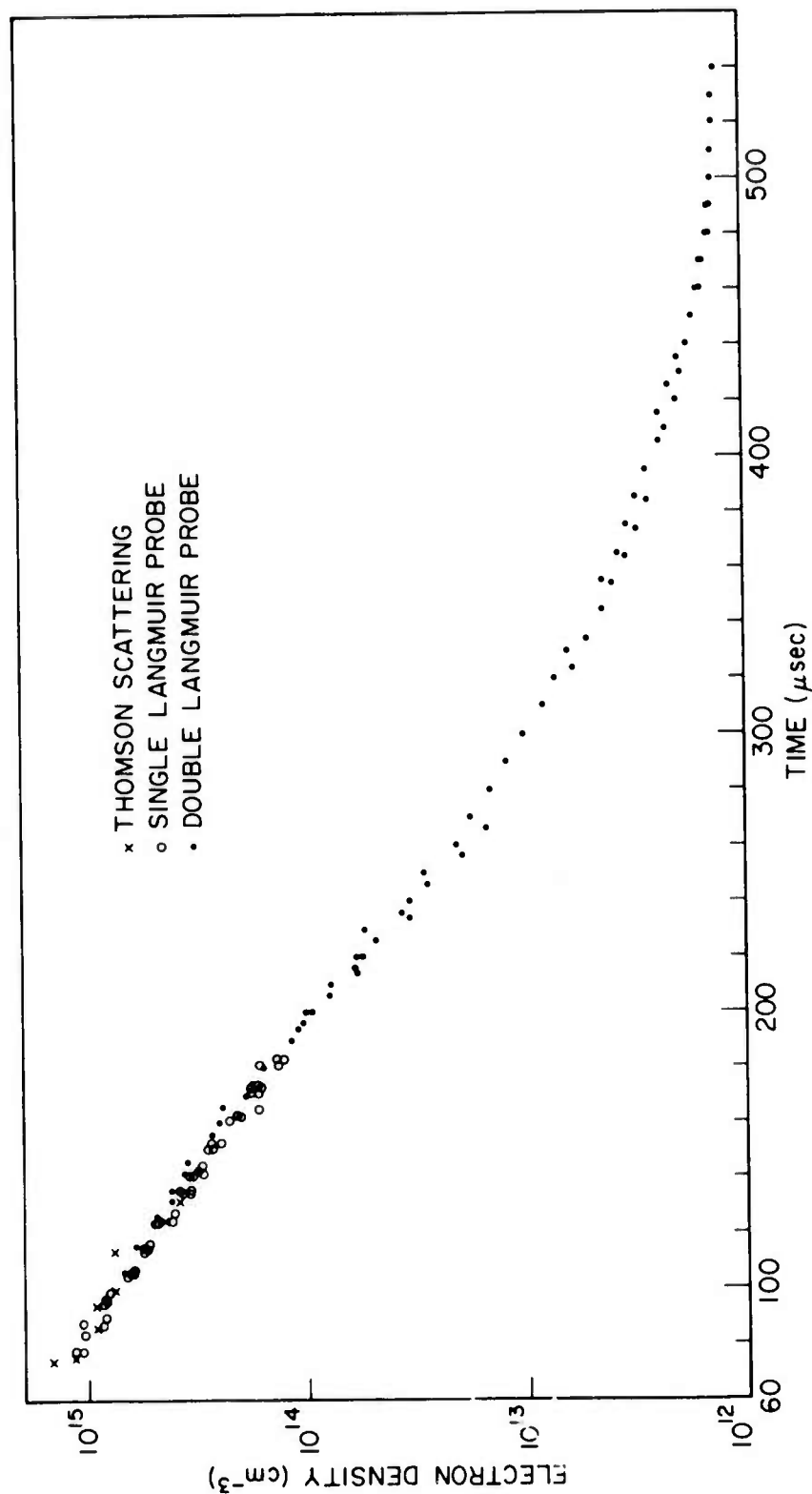
Figure 14. A plot of the electron density of the oxygen plasma versus time after initiation of main bank discharge taken on axis in the mid-plane of the single turn θ-pinch coil. The agreement between Thomson scattering and Langmuir probe techniques is seen to be good.
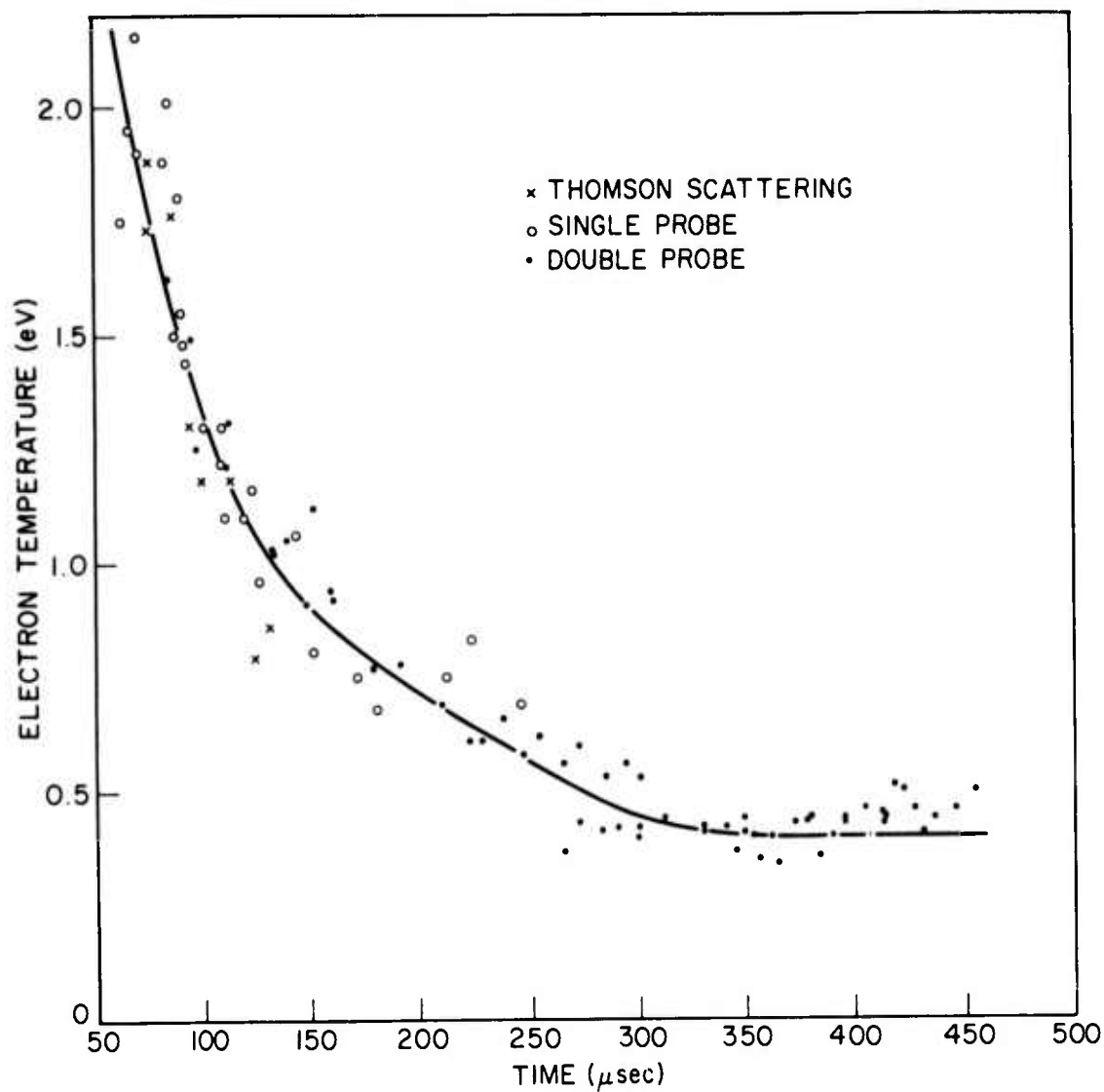
Figure 15. A plot of the electron temperature of the oxygen plasma versus time after initiation of main bank discharge taken on axis in the mid-plane of the single turn θ-pinch coil.
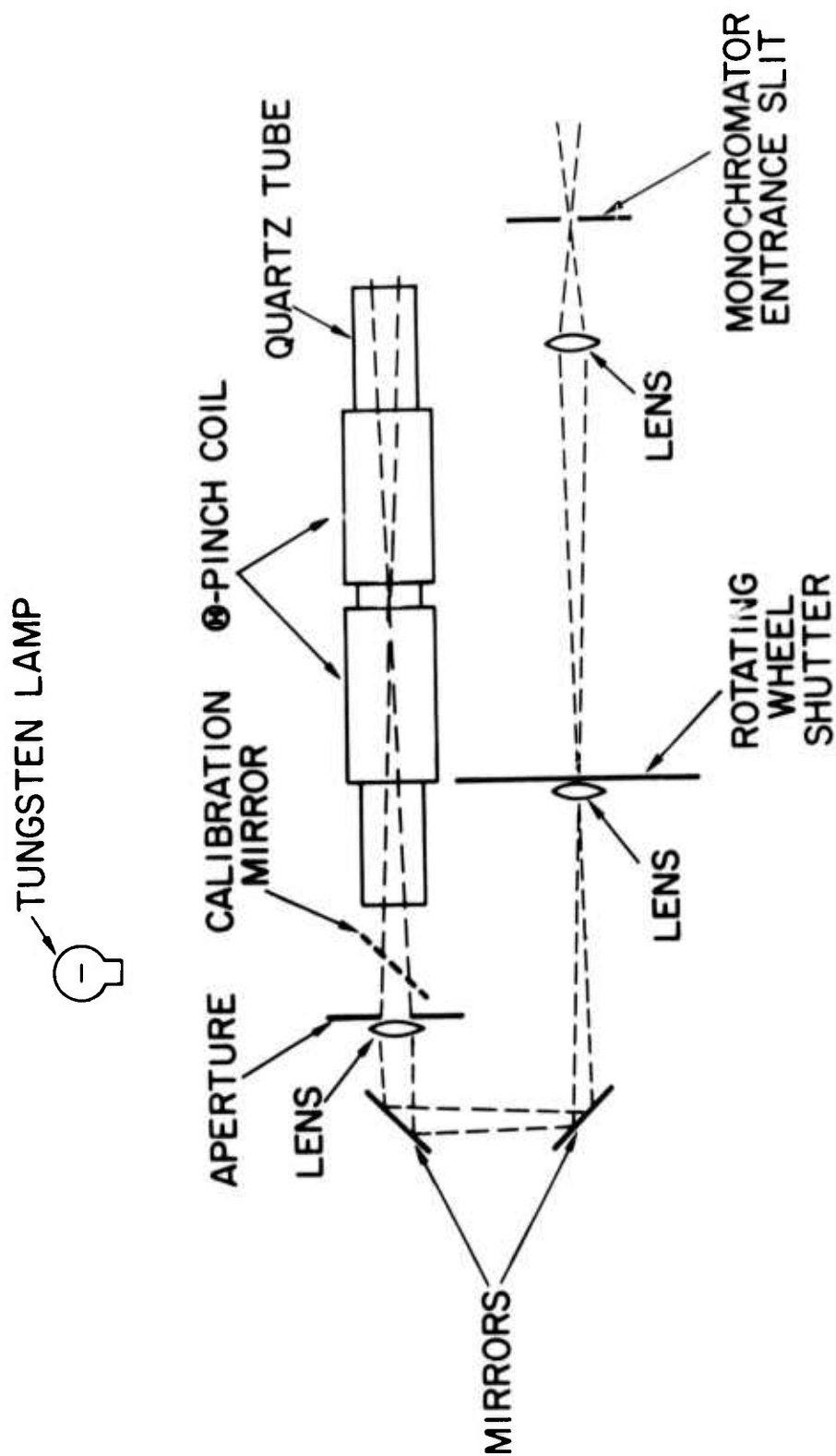
Figure 16. A schematic of the apparatus used to make absolute line intensity measurements.

25

TABLE 1. OXYGEN TRANSITIONS STUDIED

Multiplet Wavelength (Å)	Transition	Multiplet	Transition Probability $10^6(\text{sec}^{-1})$	Upper Level	
				Degeneracy	Ionization energy (eV)
5330.0	$2p^35d \rightarrow 2p^33p$	$^5D^O \rightarrow {}^5P$	1.97	25	0.554
5436.1	$2p^36s \rightarrow 2p^33p$	$^5S^O \rightarrow {}^5P$	3.05	5	0.594
6157.3	$2p^34d \rightarrow 2p^33p$	$^5D^O \rightarrow {}^5P$	7.01	25	0.854
7254.4	$2p^35s \rightarrow 2p^33p$	$^3S^O \rightarrow {}^3P$	6.20	3	0.914
6455.0	$2p^35s \rightarrow 2p^33p$	$^5S^O \rightarrow {}^5P$	7.10	5	0.954
4368.3	$2p^34p \rightarrow 2p^33s$	$^3P \rightarrow {}^3S^O$	0.66	9	1.254
3947.29	$2p^34p \rightarrow 2p^33s$	$^5P \rightarrow {}^5S^O$	0.33	15	1.328
7773.4	$2p^33p \rightarrow 2p^33s$	$^5P \rightarrow {}^5S^O$	34.00	15	2.874

Figure 17 is a plot of the experimental results obtained at 150 μsec after the initiation of main bank discharge. The number density divided by the degeneracy is plotted against the ionization energies of the various levels. At these conditions $\left[N_e \approx 2.8 \times 10^{14} \text{ cm}^{-3} \text{ and } T_e \approx 0.9 \text{ eV}\right]$, the code developed at NRL predicts populations of the energy levels should be in Saha-Boltzmann equilibrium with the free electron gas (solid line). The data, however, fits very well the population densities expected if the excited levels are in Boltzmann equilibrium with the ground state. A possible explanation for this discrepancy is that since the resonance lines are optically thick, one would expect the excited state number densities to be in Boltzmann equilibrium with the ground state (References 24 and 25). The reason the electron number density is not in equilibrium with the ground state is that there is a high electron loss rate out the ends of the containment vessel. This rate is over a factor of ten larger than the electron collisional-radiative recombination rate and tends to convert electrons plus ions into ground state atoms. This electron sink is not included in the NRL code. The error in these measurements is due almost entirely to the uncertainty of the absolute value of the atomic transition probabilities which is on the order of ~25 percent. This error estimate is confirmed, at least in a relative sense, by the small amount of scatter about the straight dashed line.

The problem now is to estimate how long it will take for these levels to relax from a Boltzmann equilibrium with the ground state to a collisional radiative equilibrium with the free electron gas once the temperature falls sufficiently to decouple the ground state. Knowing the optical depth and the excited state number densities, a time on the order of 1 μsec was estimated to be sufficient for the triplet system whereas the relaxation of the quintet system would depend on the rate of spin exchange collisions. As can be seen from Figures 18 and 19, the relaxation time is more like 50 to 100 μsec and both the quintet and triplet systems tend to relax at roughly the same rate. The reason for the slow decay rate is not understood, but the equality of the triplet and quintet decay rates indicates a large spin exchange rate. It also is apparent from the figures that for times larger than 300 μsec after initiation of main bank discharge the populations of the excited states will be determined by a collisional radiative model and will not be radiatively tied to the ground state.

The experimentally determined number densities of eight levels as a function of ionization energy are shown for 300 μsec after initiation of main bank discharge in Figure 20. Figure 21 contains a similar plot for seven levels at 350 μsec after initiation of main bank discharge. The uncertainties of the individual level number

27
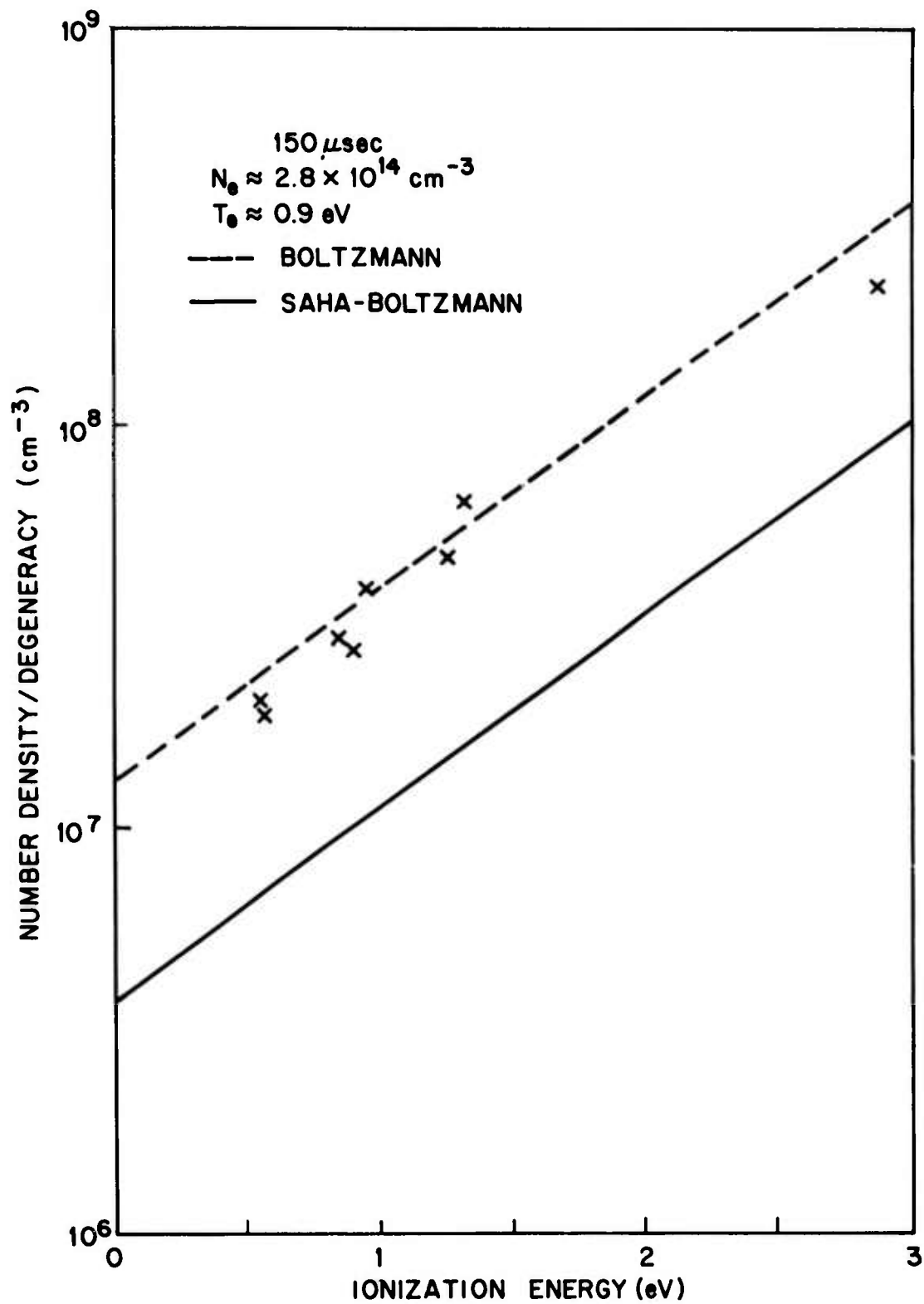
Figure 17. Experimental results at 150 μsec after initiation of main bank discharge in the oxygen plasma.
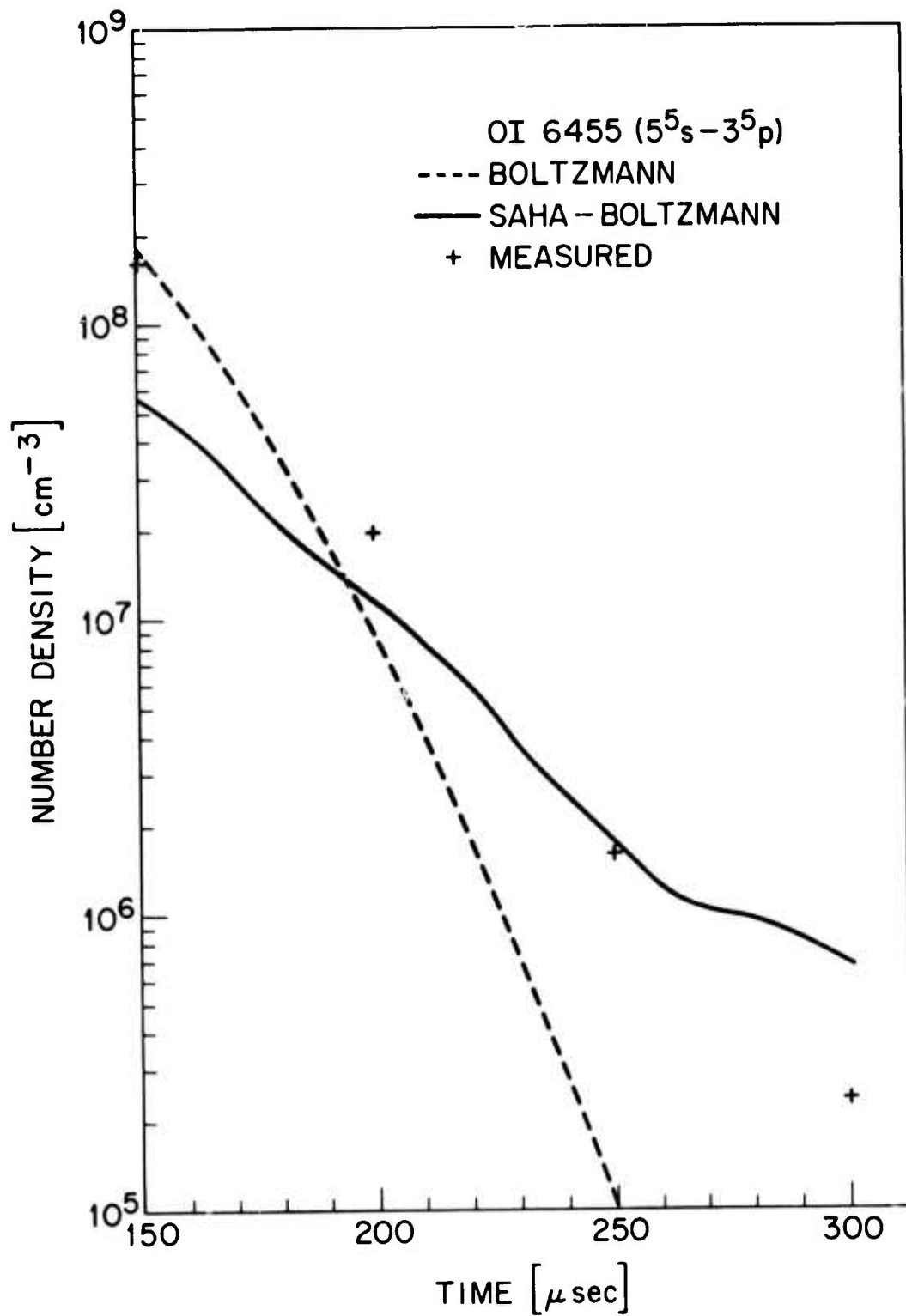
Figure 18. Time development of the number density of the atomic oxygen 5^5s level.
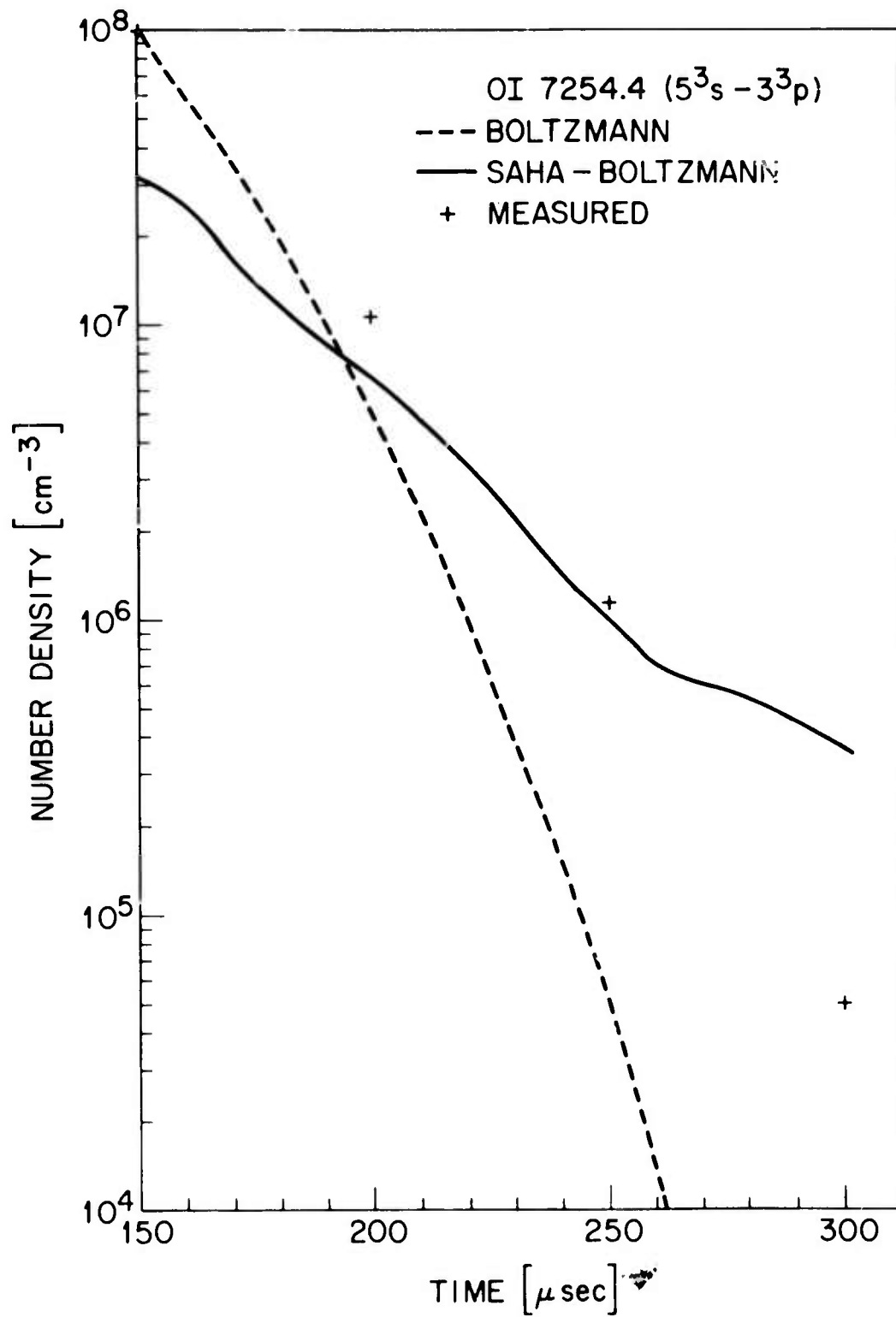
Figure 19.   Time development of the number density
of the atomic oxygen 5^3s level.

30
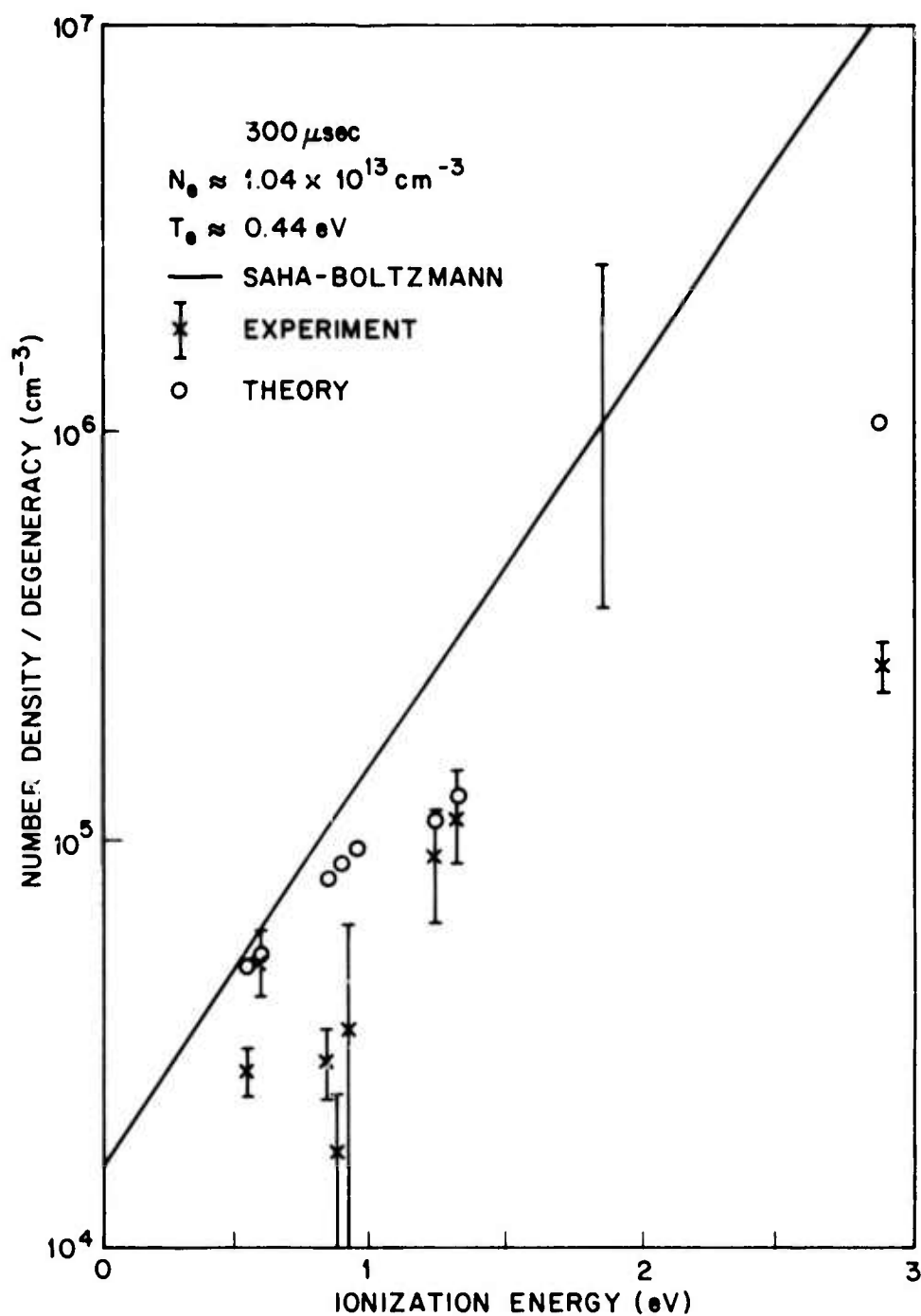
Figure 20. Comparison of experimental $\left(\begin{smallmatrix} \mathrm{I} \\ * \\ \mathrm{I} \end{smallmatrix}\right)$ number densities of oxygen excited states divided by their degeneracies with calculated values (0) at 300 μsec after initiation of main bank discharge.

31
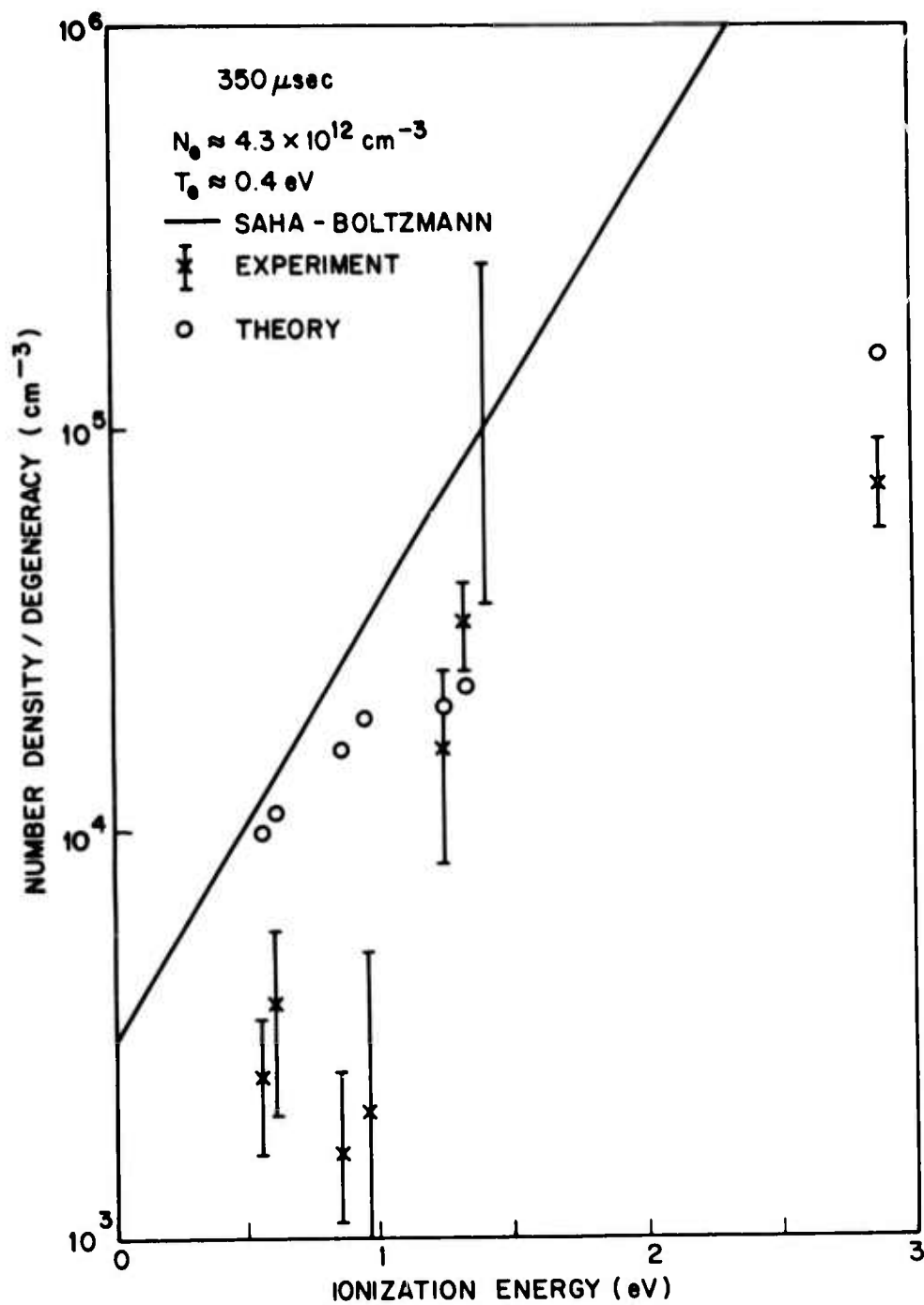
Figure 21. Comparison of experimental $\left(\underset{\text{I}}{\overset{\text{I}}{\text{X}}}\right)$ number densities of oxygen excited states divided by their degeneracies with calculated values (0) at 350 μsec after initiation of main bank discharge.

32

density measurements due to measurement error alone are indicated by the error bars on the experimental points. The error bar on the solid line in each figure represents the amount of change which can be obtained in the collisional model by changing the electron temperature and density to their extreme measured values. The number densities calculated from the NRL computer program are also shown in the figures. The program uses Seaton type cross-sections for collisional excitation and de-excitation between all levels with dipole allowed transitions; i.e., n, $\ell + 1$, even spin exchange collisions. If spin exchange collisions are ignored, the calculated number density for the 3^5p level is almost two orders of magnitude too high. This indicates that the 3^5s level is not metastable at these conditions and can be collisional depopulated to the triplet system (References 26 and 27). It also should be noted that the measured number densities are considerably lower than those calculated for the levels which have an ionization energy between 0.9 and 1.0 eV. The explanation for this discrepancy may be that the code does not take into account the influence of core excited states. The 3s' ^1D level is nearly degenerate with the levels in question and can be depopulated rapidly by an optically thin radiative transition to the 2p ^1D level. This may mean that the 3s' ^1D level acts like a sink which will tend to depopulate the levels with nearly the same energy.

IV. NITROGEN MEASUREMENTS

A. Diagnostics

The ambient fill gas used throughout this part of the experiment was pure N_2 at a pressure of 10 mTorr. As with the oxygen work discussed in the previous section, the first diagnostic undertaken in nitrogen was to take the visible spectrum shown in Figure 22. The upper spectrum on each strip is neon spectrum used for wavelength calibration. The lower spectrum on each strip shows the neutral and ionized lines of the nitrogen atom clearly. Besides these, however, the strong bands of the neutral (N_2) and singly ionized molecule (N_2^+) can also be seen. Of course nitrogen is well known for having strong molecular band emission in the visible part of the spectrum (Reference 28). The only lines found which were not associated with nitrogen were the lines of the hydrogen Balmer series. This indicates a high degree of purity in the plasma.

The time development of the various species present (N, N^+, N_2, and N_2^+) was investigated. It was found that the N^+, N_2, and N_2^+ emission occurred only during the first 50 μsec of the discharge and after that the emission from the neutral atomic nitrogen lines predominated. Of course the N_2 emission bands
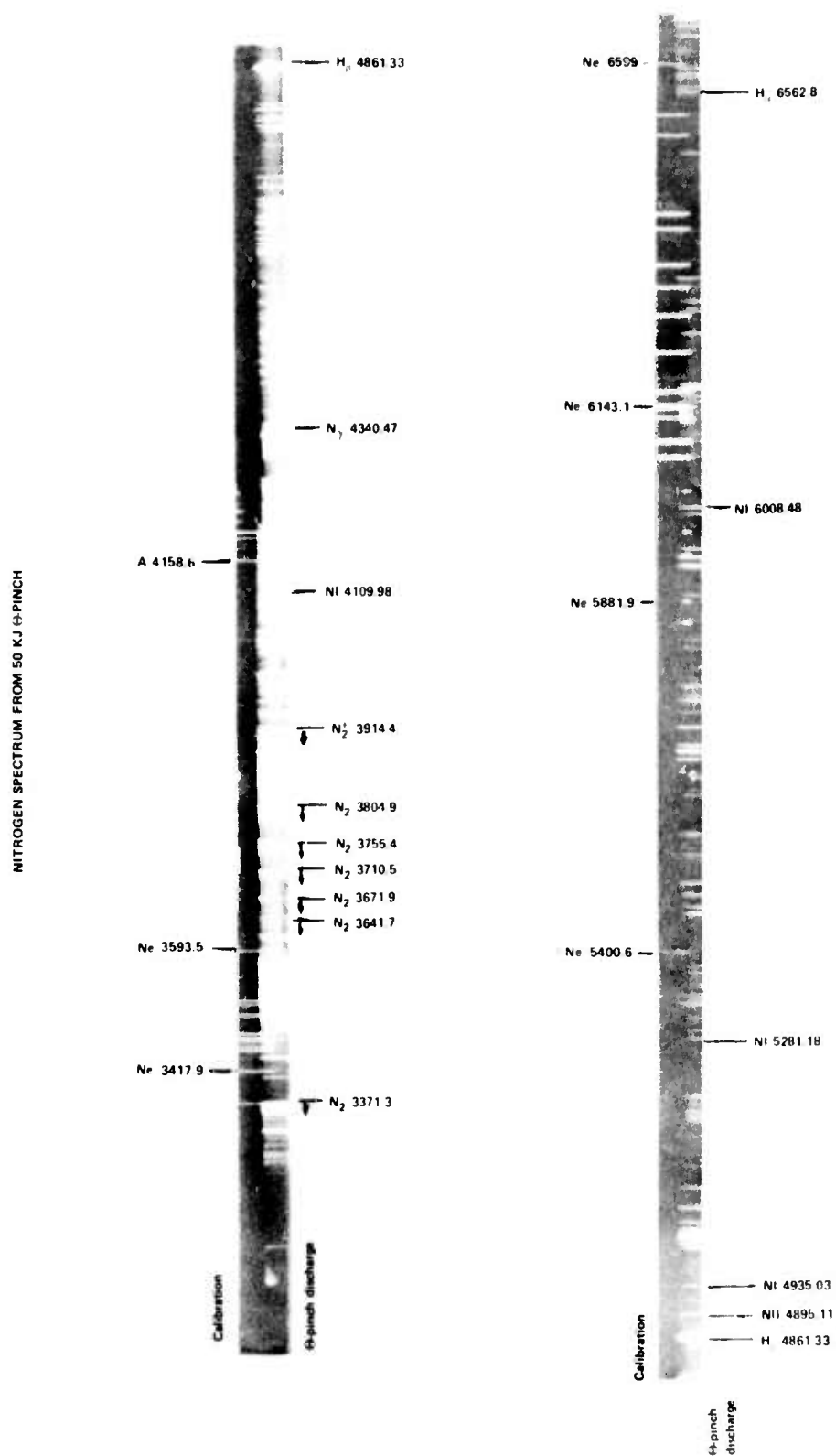
33

Figure 22. Time integrated spectrum of visible light
emitted from the nitrogen plasma.

must also occur very late in the afterglow, but this emission was not observed on the time scale of this experiment.

As in the previously described oxygen work, the spatial development of the nitrogen plasma as a function of time after the initiation of main bank discharge was investigated with the double Langmuir probe. The temperature was again found to be constant over the spatial coordinates and vary only with time. The relative ion density was measured as a function of radial position for various times after the initiation of main bank discharge at the mid-plane of the single turn main coil. A plot of the results of this measurement is shown in Figure 23. As can be seen, the density distribution is not quite as homogeneous as in the oxygen case, however, it is still felt that as long as the end-on viewing aperture is held down to 4 cm there will be no need for radial homogeneity corrections.

The axial variation of ion density as a function of time after main bank discharge was also investigated with the free running double Langmuir probe. Figure 24 is a plot of ion saturation current (proportional to ion density) as a function of axial position for various times after main bank discharge. As can be seen, the ion density is very nearly constant inside the main coil (0 to 40 cm) and falls off somewhat faster at the later times outside the coil than the oxygen plasma did. The nitrogen plasma, as did the oxygen plasma, also displays an ion density increase at the end of the main coil ~ 250 μsec after the initiation of main bank discharge. This increase is probably due to a reflected shock wave returning from the end wall of the plasma tube.

An effective length, ℓ_{eff}, was also calculated for this plasma in the same way as was done for the oxygen plasma. A plot of ℓ_{eff} versus time after the initiation of the main bank discharge is shown in Figure 25. As can be seen, the plasma effective length tends to just be the main coil length of 80 cm at the later times.

The electron temperature and ion density were measured on the axis of the discharge tube in the mid-plane of the main turn coil. Plots of the electron temperature and ion density as functions of time after the initiation of main bank discharge are shown in Figures 26 and 27. On the same graphs we have also plotted a Thomson scattering measurement of the electron temperature and density done 100 μsec after the initiation of main bank discharge. The Thomson scattering value of the electron temperature is only about 12 percent lower than the Langmuir probe measured value. For electron density Thomson scattering gives a value about 20 percent lower than found from the Langmuir probe work. These small discrepancies are within the scatter of experimental error and thus
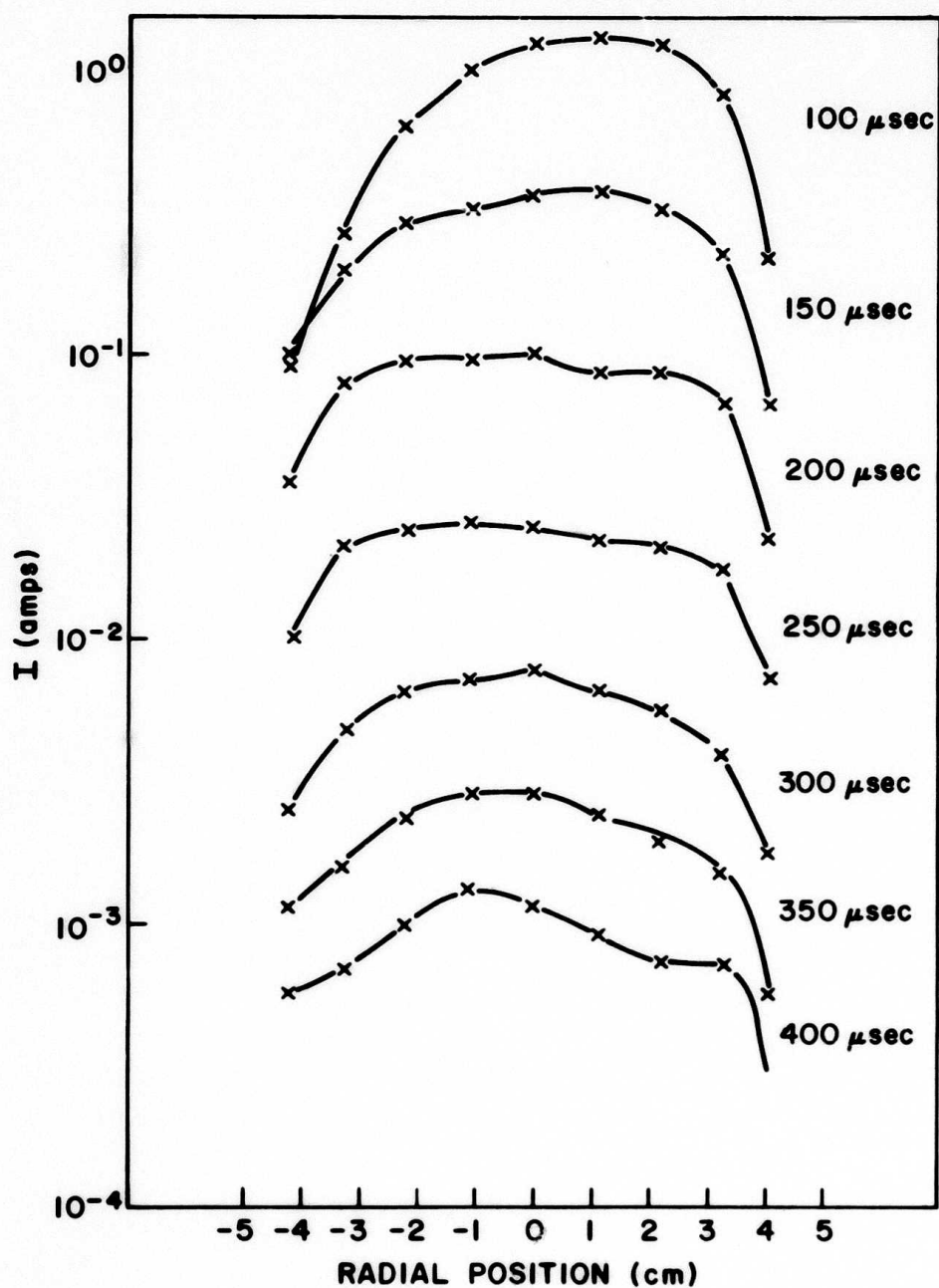
Figure 23. Scan of the ion saturation current versus radial position as a function of time after the initiation of main bank discharge. These scans were taken in the nitrogen plasma in the mid-plane of the single turn θ-pinch coil.

36
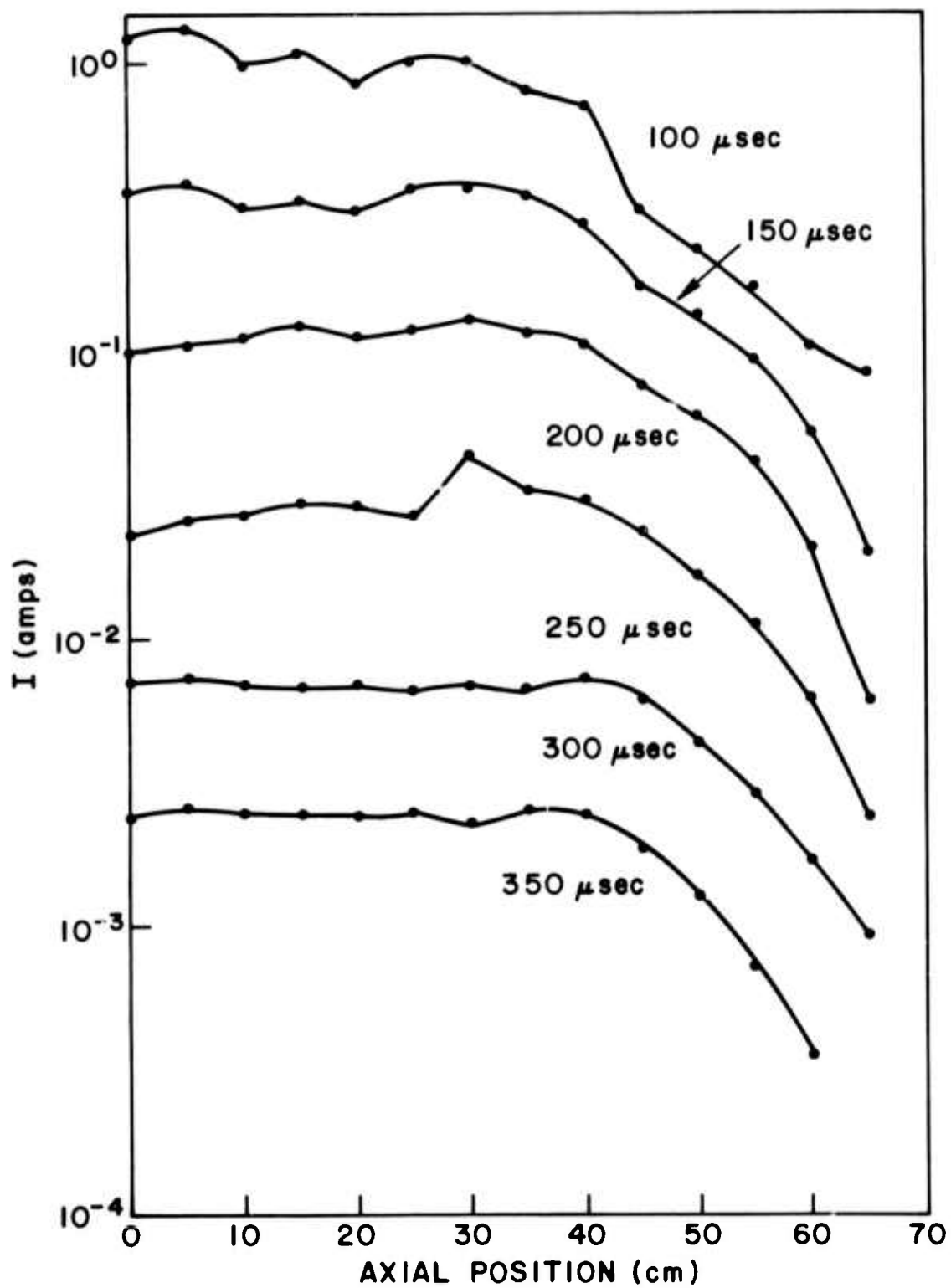
Figure 24. A plot of ion saturation current versus axial position for the nitrogen plasma at various times after the initiation of main bank discharge.
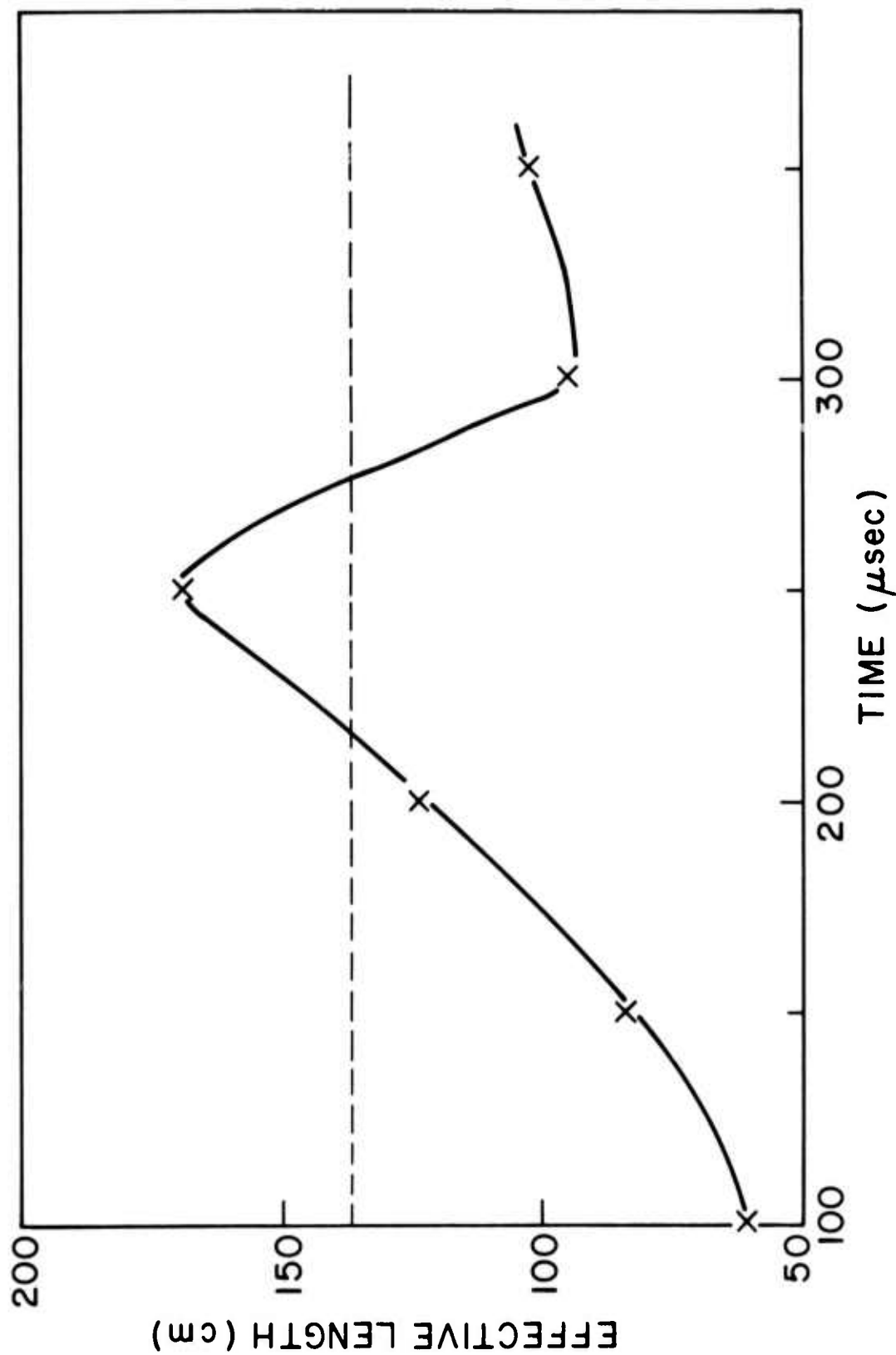
Figure 25. A graph showing the variation of the effective length of the oxygen plasma as a function of time. The dashed line is the length of the quartz containment tube.

38

Figure 26. A plot of the electron temperature of the nitrogen plasma versus time after the initiation of main bank discharge taken on axis in the mid-plane of the single turn θ-pinch coil.

Figure 27. A plot of the electron density of the nitrogen plasma versus time after the initiation of main bank discharge taken on axis in the mid-plane of the single turn θ-pinch coil.

40

the two methods again show very good agreement. In what follows the electron temperature and density will be used as measured by the Langmuir probe.
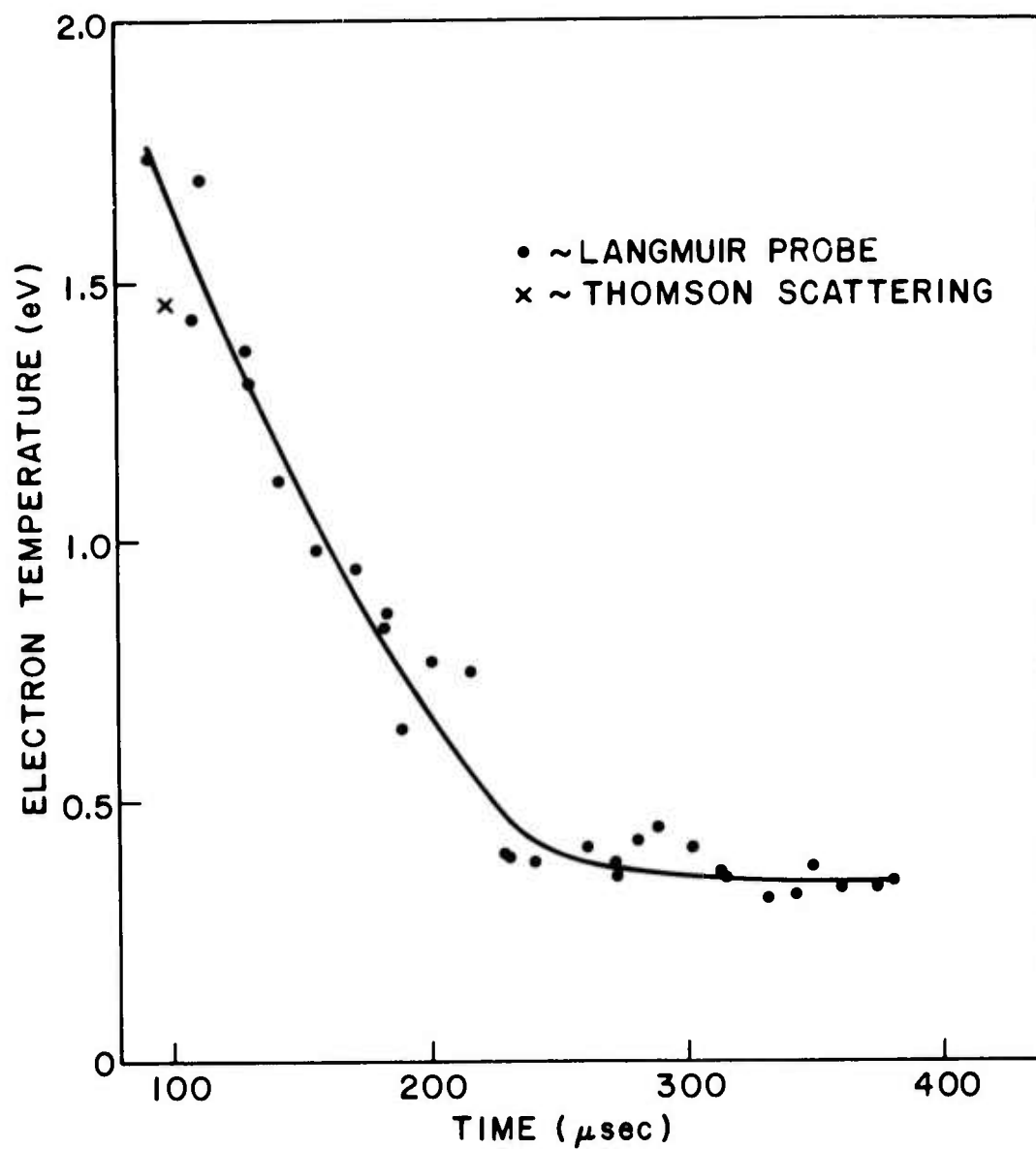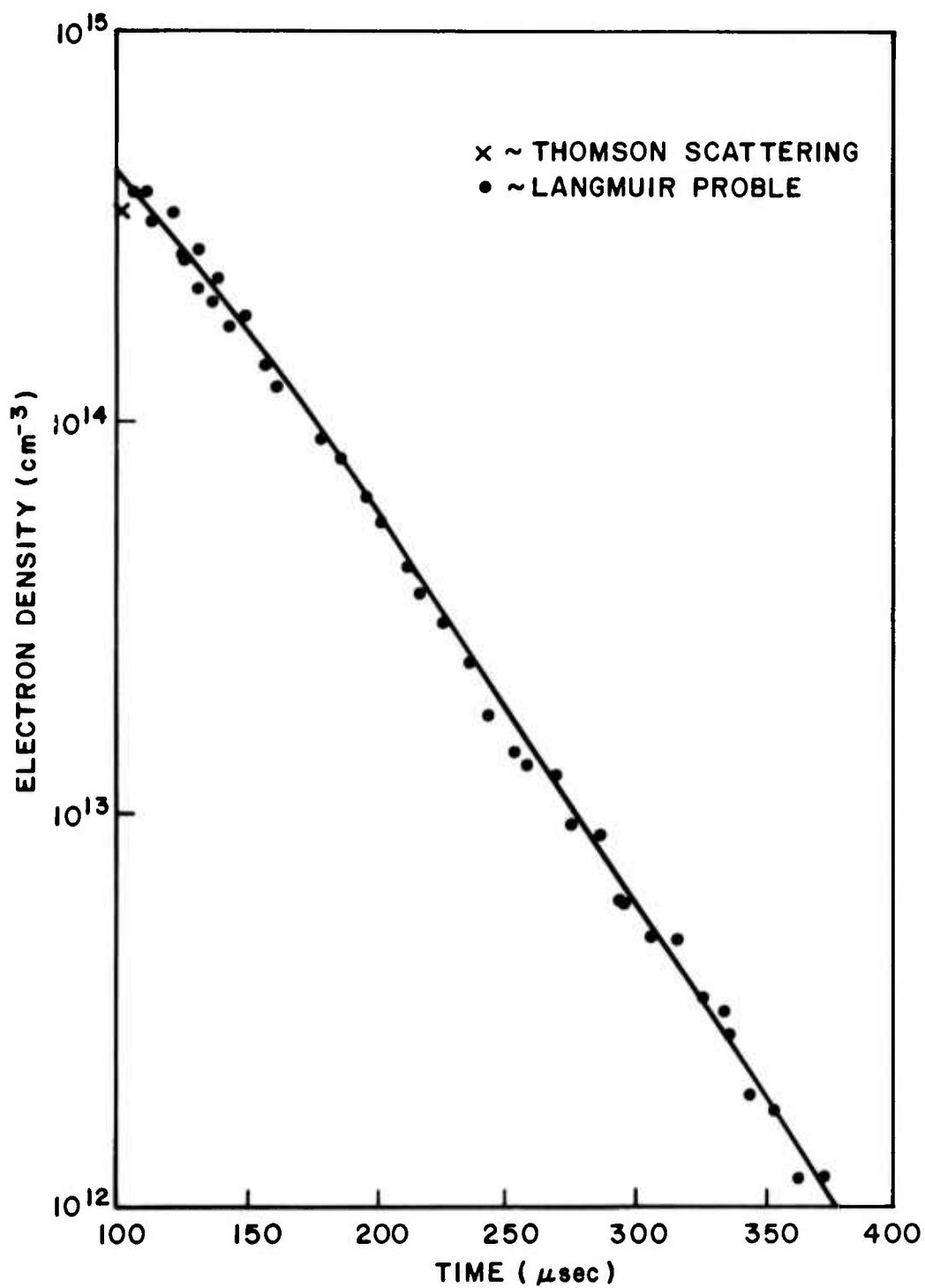
B. Results

Absolute intensity measurements of eight neutral nitrogen multiplets were made on the same apparatus used to take the previously described oxygen data, Figure 16. Table 2 gives the wavelengths, transitions, upper state degeneracies and ionization energies, and the atomic transition probabilities of the bound-bound radiation measured (Reference 23). The number density divided by the degeneracy of the upper levels of these eight transitions are shown at 150 μsec, 200 μsec, 250 μsec, 300 μsec, and 350 μsec after the initiation of main bank discharge in Figures 28 through 32.

Note should first be taken of the multiplet produced by the 4p $\rightarrow$ 3s ($^4P^O \rightarrow {}^4P$) transition shown in Figure 28 as a low point. The value of the atomic transition probability for this transition as published in Wiese, et al., is a factor of ten too large (Reference 29). As can be seen in the figure, a much better agreement is obtained when the number density of the upper level of this transition is multiplied by ten. In Figures 29 through 31, this correction has been carried out, but not indicated. The uncertainty in the transition probabilities for these eight nitrogen transitions is about 50 percent, as opposed to $\sim$25 percent for the oxygen transitions measured, and this larger uncertainty is indicated by the larger scatter about the theoretical curve in Figure 28.

The next thing to notice about the 150 μsec measurements is that, as in the case of the oxygen studies, the ground state is over-populated. However, in this case, the ground state is over-populated by about a factor of 500 instead of the factor of 3 found for oxygen. This is due to the higher electron temperature and density of the nitrogen plasma. When one uses the ground state over-population factor along with the measured temperature to interpolate between the curves published by Park (Reference 25) from his radiative-collisional non-equilibrium calculation on nitrogen one obtains the dashed line on Figure 28. The good agreement is rather fortuitous since a small error in the plasma temperature will make a large difference in the calculated over-population of the ground state. When a reasonable error is allowed in the temperature measurements made at 200 μsec after the initiation of main bank discharge, one finds that the data at this time is also consistent with the calculations done by Park.

A problem arises when the measurements 250 μsec, 300 μsec, and 350 μsec after main bank discharge are considered. The ground state is several orders of magnitude under-populated at those times relative to the equilibrium population

41

TABLE 2. NITROGEN TRANSITIONS STUDIED

Multiplet Wavelength (Å)	Transition	Multiplet	Transition Probability $10^6 (\sec^{-1})$	Upper Level	
				Degeneracy	Ionization energy (eV)
5201.80 5197.80	$2p^2 5d \rightarrow 2p^2 3p$	$^2P \rightarrow {}^2S^o$	2.30	6	0.547
6646.51 6644.96	$2p^2 5s \rightarrow 2p^2 3p$	$^4P \rightarrow {}^4D^o$	2.82	8	0.908
6981.80 6979.10	$2p^2 5s \rightarrow 2p^2 3p$	$^4P \rightarrow {}^4P^o$	1.21	6	0.915
4151.46	$2p^2 4p \rightarrow 2p^2 3p$	$^4S^o \rightarrow {}^4P$	1.30	4	1.210
4224.74 4223.04 4222.12 4218.87	$2p^2 4p \rightarrow 2p^2 3s$	$^4P^o \rightarrow {}^4P$	4.09*	12	1.270
4935.03	$2p^2 4p \rightarrow 2p^2 3s$	$^2S^o \rightarrow {}^2P$	1.58	2	1.330
7468.31	$2p^2 3p \rightarrow 2p^2 3s$	$^4S^o \rightarrow {}^4P$	16.10	4	2.660
8188.01 8184.85	$2p^2 3p \rightarrow 2p^2 3s$	$^4P^o \rightarrow {}^4P$	7.46	10	2.690

* This transition probability as recorded in Reference 22 is a factor of 10 too high.

Figure 28. A plot of the experimental number densities of nitrogen excited states divided by their degeneracies versus their ionization energies at 150 μsec after the initiation of main bank discharge.

43

Figure 29. A plot of the experimental number densities of nitrogen
excited states divided by their degeneracies versus
their ionization energies at 200 μsec after the initiation
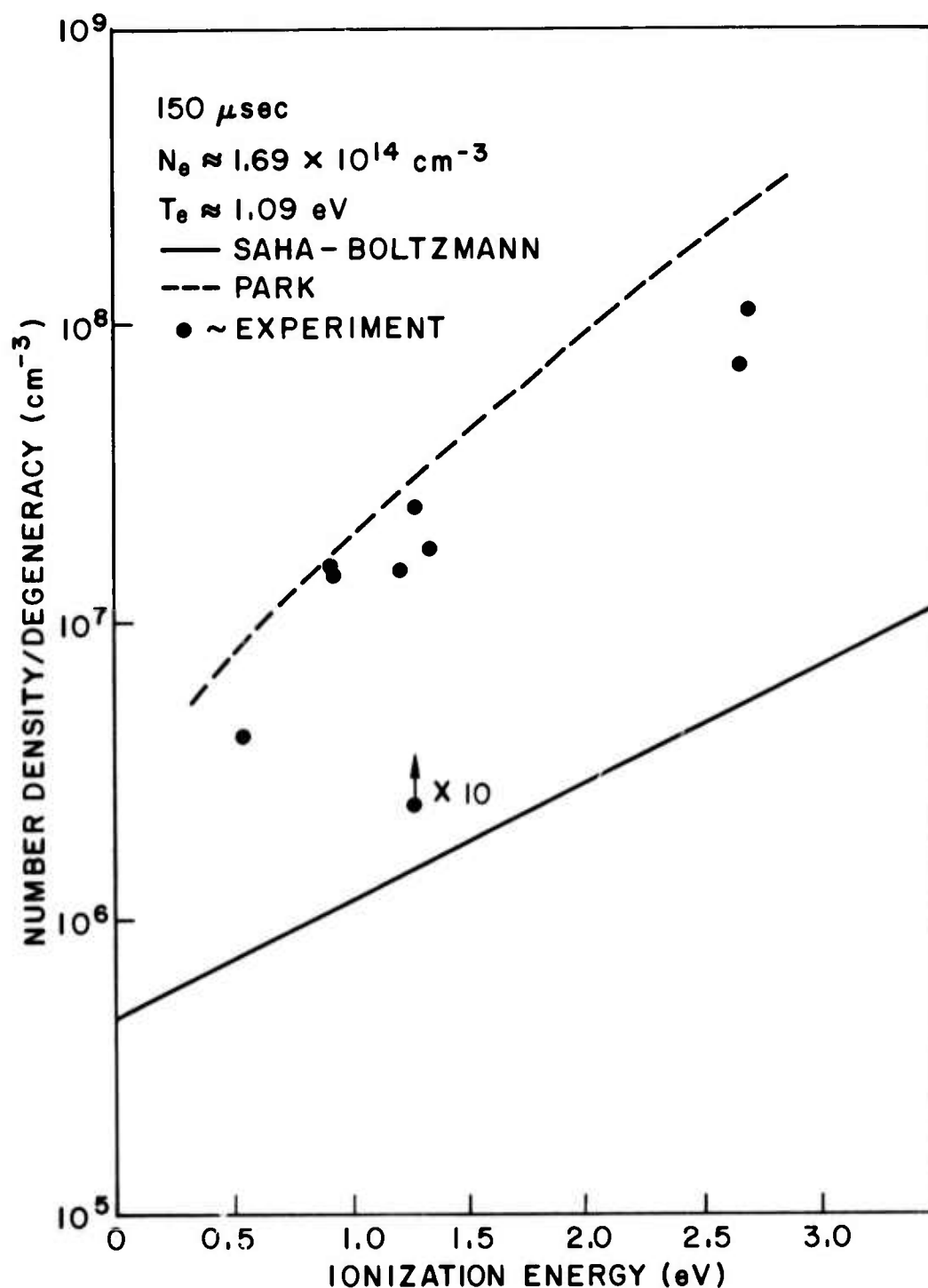of main bank discharge.

44

Figure 30. A plot of the experimental number densities of nitrogen excited states divided by their degeneracies versus their ionization energies at 250 μsec after the initiation of main bank discharge.

Figure 31. A plot of the experimental number densities of nitrogen excited states divided by their degeneracies versus their ionization energies at 300 μsec after the initiation of main bank discharge.
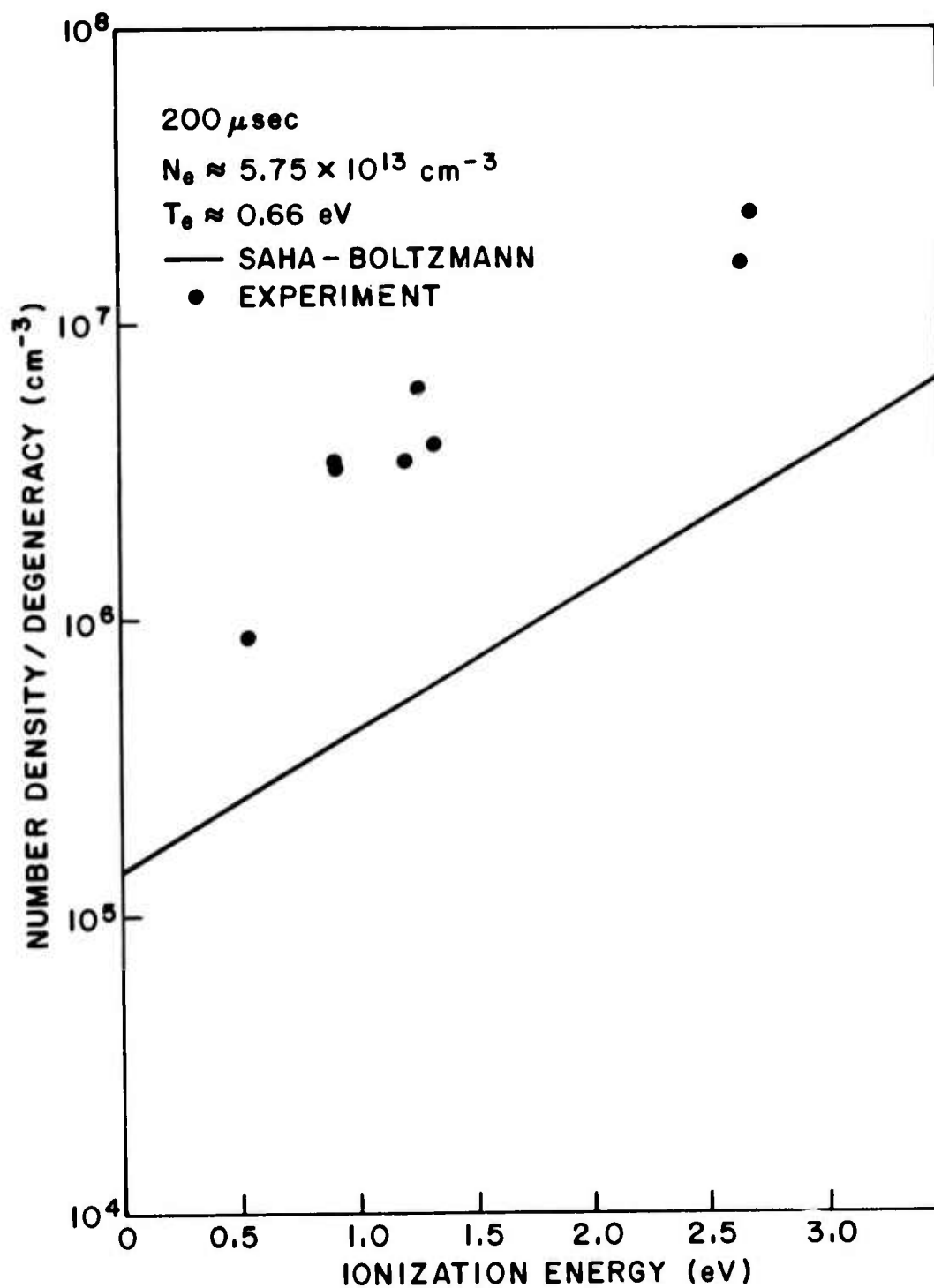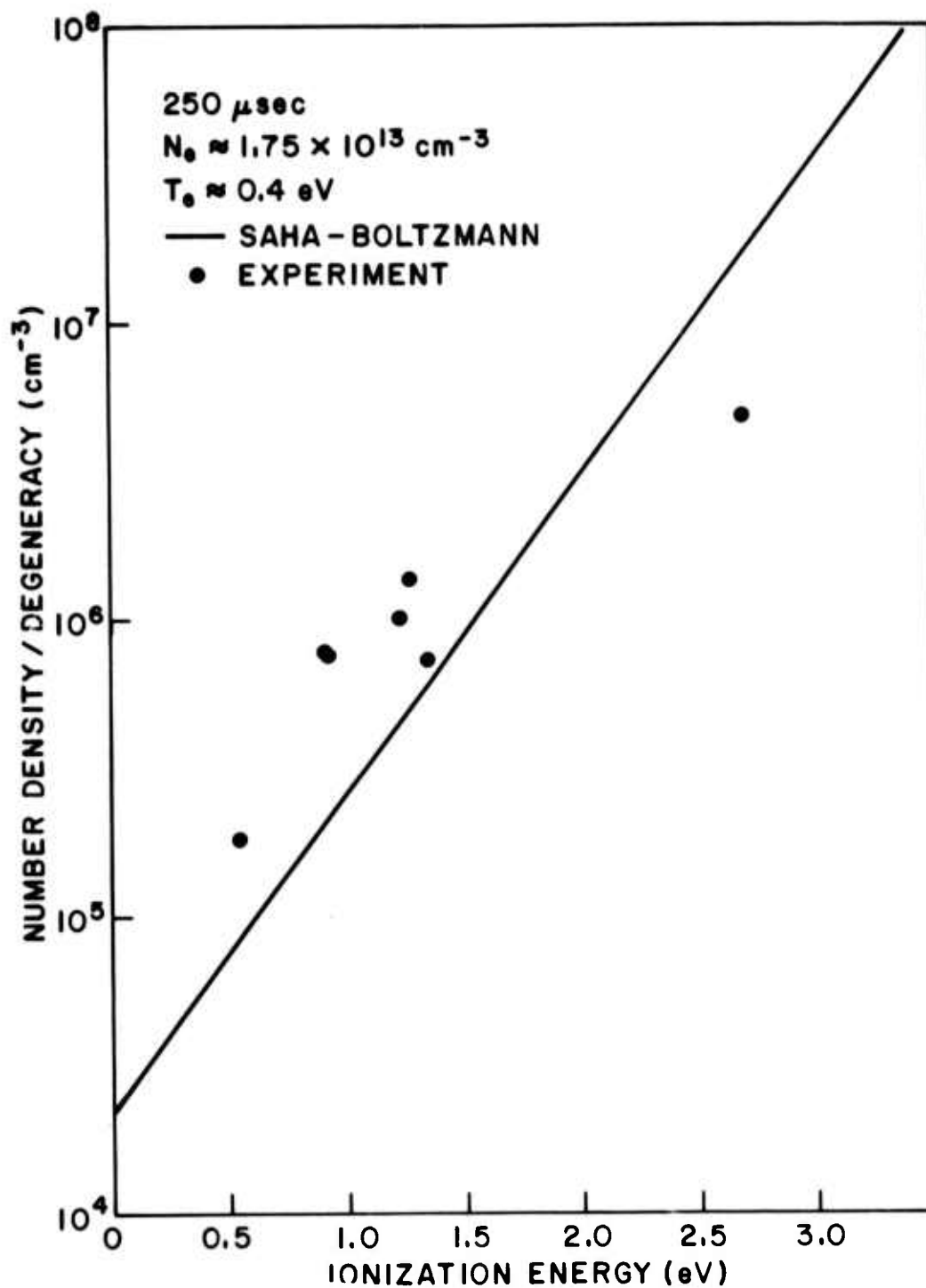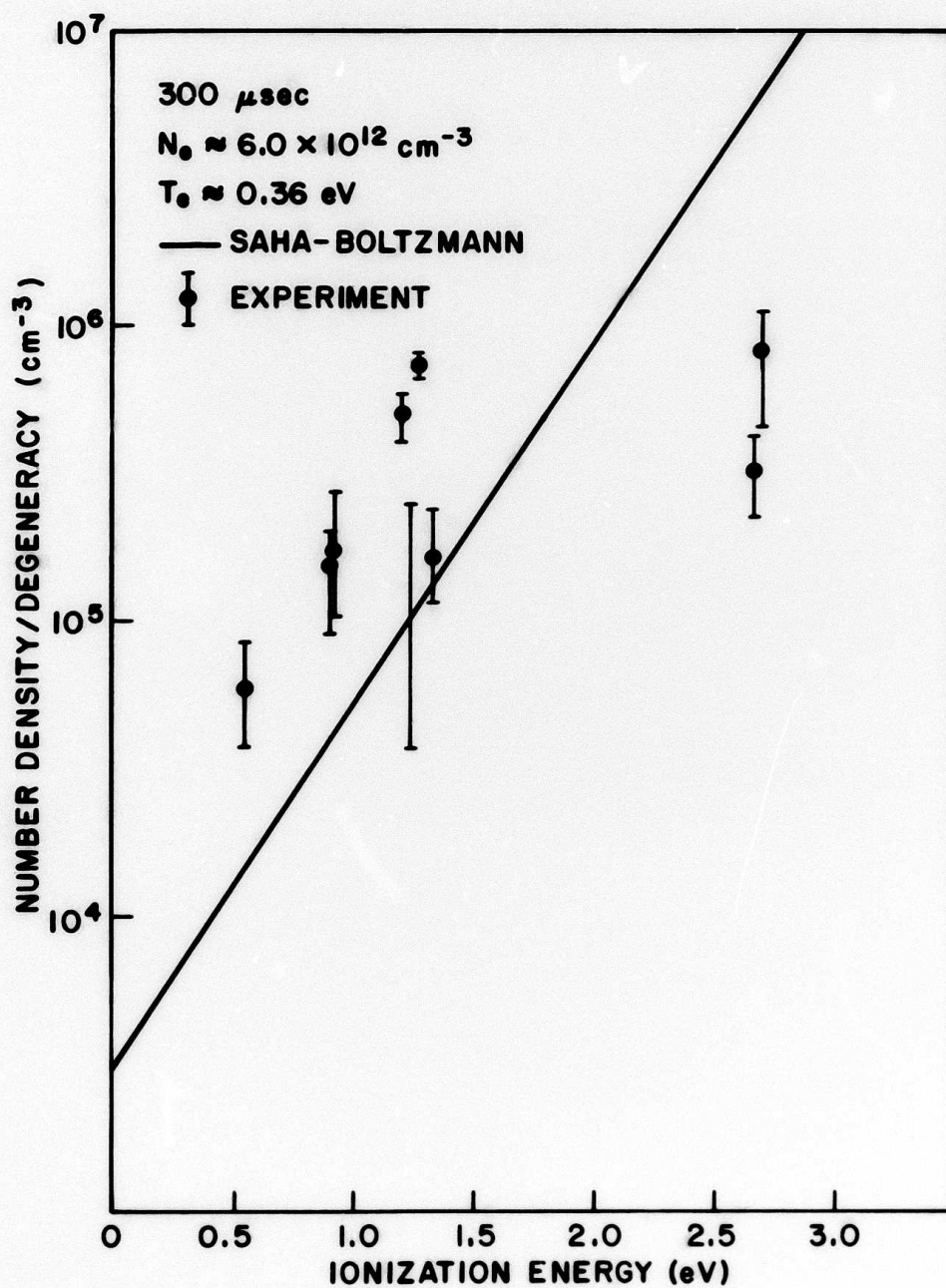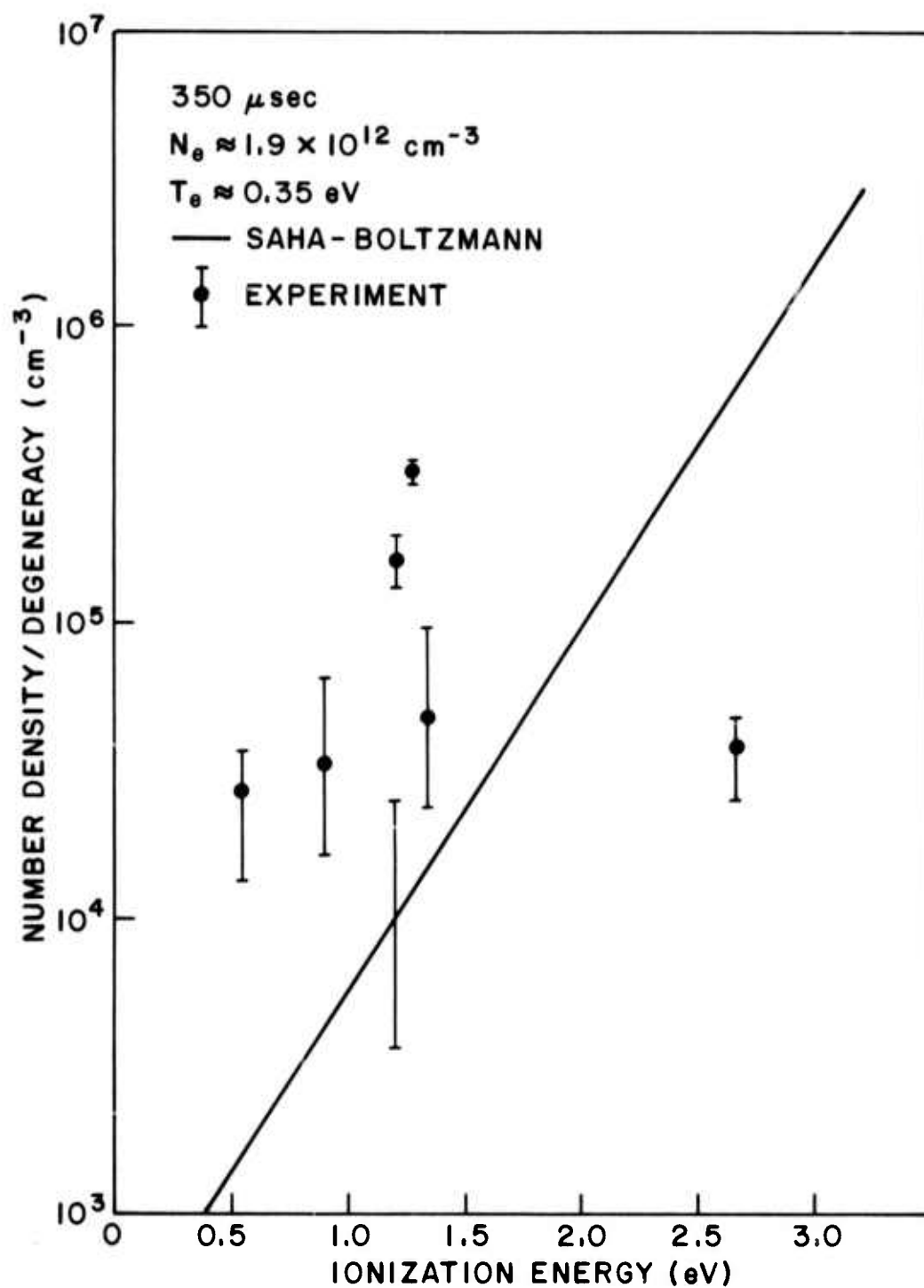
46

Figure 32. A plot of the experimental number densities of nitrogen excited states divided by their degeneracies versus their ionization energies at 350 μsec after the initiation of main bank discharge.

and the levels measured should fall below the Saha-Boltzmann line drawn on the plots. However, as can easily be seen, the levels are over-populated and this trend gets larger at later times. This effect seems real since the discrepancy lies outside the indicated errors on the measurements, and even invoking the 50 percent uncertainty on the individual transition probabilities does not bring agreement. This observation indicates that some reaction is occurring which supplies excited state nitrogen atoms at a higher rate than collisional-radiative recombination. One possible energetic reaction is $N + N + N \rightarrow N_2 + N^*$ where N^* indicates an excited nitrogen atom. In order for this reaction to compete with electron radiative-collisional recombination, it must have a rate coefficient on the order of 3×10^{-17} cm^3/sec. This is a bit larger than presently accepted but other energetically possible reactions fall much farther short of the needed rate.

Another possibility that was considered was that the Langmuir probe introduced impurity oxygen into the nitrogen plasma thereby lowering the electron density at the late times through the reactions

$$N^+ + O_2 \rightarrow N + O_2^+$$

and

$$O_2^+ + e \rightarrow O_2 \quad .$$
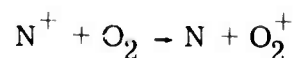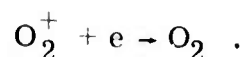
Then when measurements of the absolute line intensity were made, without the probe being present, the electron density was higher. This explanation can only be true if radiative-collisional recombination through the impurity channel controls the electron loss rate in the plasma. The electron loss rate for this plasma is completely dominated (by several orders of magnitude) by the flow of electrons and ions out the open ends of the θ-pinch tube. This means that even the addition of a large amount of impurity would not affect the electron density of the plasma.

V. SUMMARY

The early time, ($N_e \approx 10^{14}$ cm^{-3} $T_e \approx 1$ eV) oxygen and nitrogen results are well understood when the over-population of the ground state is taken into consideration. The early time nitrogen results agree very well with the calculations done by Park, but the NRL radiative-collisional recombination code does not seem to give the correct results in this limit for oxygen.

At late times, ($N_e \approx 10^{12}$ cm^{-3}, $T_e \approx 0.4$ eV) the NRL code gives good agreement with the oxygen experiment if large collisional spin exchange cross-sections are used. However, the NRL code does not reproduce the experimentally

observed under-population of the levels with ionization energies of ~ 0.9 eV since it does not take into account the depopulizing effect of the 3s' ^{1}D level. The late time behavior of the nitrogen plasma is not well understood at this time (Reference 30). However, since the discrepancy is larger than can be accounted for by probable experimental inaccuracies, we believe it to be real.

LIST OF REFERENCES

1. Julienne, P.S., Davis, J., and Hyman, E. "Departure From LTE in an Oxygen Plasma." Naval Research Laboratory Memorandum Report 2740, March 1974.

2. Sappenfield, D. Personal Communication, 1969.

3. Drawin, H.W. and Emard, F. Z. Physik 254, 202, 1972.

4. Drawin, H.W. Z. Physik 225, 470, 1969.

5. Bates, D.R. and Kingston, A.E. Planet. Space Sci. 11, 1, 1963.

6. Bates, D.R., Kingston, A.E., and McWhirter, R.W.P. Proc. Roy. Soc. A267, 297, 1962.

7. Seaton, M.J. "Atomic and Molecular Processes." ed. by D.R. Bates. (Academic Press, New York and London, 1962), Chapter 11.

8. Griem, Hans R. "Plasma Spectroscopy." McGraw-Hill, New York, 1964.

9. Johnson, L.C. and Hinnov, E. Phys. Rev. 187, 143, 1969.

10. Hinnov, Einar. Phys. Rev. 147, 197, 1966.

11. Hinnov, Einar and Hirschberg, Joseph G. Phys. Rev. 125, 795, 1962.

12. Smith, D. and Plumb, I.C. J. Phys. D. 5, 1226, 1962.

13. Goodall, C.V. and Smith, D. Plasma Phys. 10, 249, 1968.

14. Waymarth, John F. J. Appl. Phys. 37, 4492, 1966.

15. Cohen, Ira M. Phys. Fluids 13, 889, 1970.

16. Irisana, J. and John, P.K. Rev. Sci. Instrum. 44, 102, 1973.

17. Chen, Francis F. "Plasma Diagnostic Techniques." ed. by R.H. Huddlestone, and S.L. Leonard. (Academic Press, New York, 1965), Chapter 4.

18. Chang, Jen-Shih. J. Phys. D 6, 1674, 1973.

19. Schott, L. "Plasma Diagnostics." ed. by W. Lochte-Holtgreven, (North-Holland, Amsterdam, 1968), Chapter 11.

20. Bohm, D. "The Characteristics of Electrical Discharges in Magnetic Fields." ed. by A. Guthrie and R.K. Wakerling. McGraw-Hill, New York, 1949.

21. Kunze, H.J. "Plasma Diagnostics." ed. by W. Lochte-Holtgreven, (North-Holland, Amsterdam, 1968), Chapter 9.

22. DeSilva, A.W. and Goldenbaum. G.C. "Methods of Experimental Physics." Vol. 9 - Part A, ed. by H.R. Griem and R.H. Lovberg (Academic Press, New York and London, 1970), Chapter 3.

LIST OF REFERENCES (Continued)

23. Wiese, W.L., Smith, M.W., and Glennon, B.M. "Atomic Transition Probabilities." Nat. Bur. Stand., Washington, D.C., 1966.
24. Engelhardt, E. Physics of Fluids 16, 217, 1973.
25. Park, C. Quant. Spectrosc. Radiat. Transfer, 8, 1633, 1968.
26. Burrell, C.F. and Kunze, H.J. Phys. Rev. Letters 28, 1, 3 January 1972.
27. Ojha, S.P., Tiwari, P., and Rai, D.K. J. Phys. B 5, 2271, 1972.
28. Anketell, J. and Nicholls, R.W. Rep. Prog. Phys., 33, 269, 1970.
29. Motschmann, Harold. Z. Für Physik. 143, 77, 1955.
30. Tunistskii, L.N. and Cherkasov, E.M. 13, 1696, 1969.